# ANISOTROPY OF THERMOELECTRIC POWER IN BISMUTH TELLURIDE

JANE HODGSON DENNIS

TECHNICAL REPORT 377

JANUARY 15, 1961



MASSACHUSETTS INSTITUTE OF TECHNOLOGY
RESEARCH LABORATORY OF ELECTRONICS
CAMBRIDGE, MASSACHUSETTS

The Research Laboratory of Electronics is an interdepartmental laboratory of the Department of Electrical Engineering and the Department of Physics.

The research reported in this document was made possible in part by support extended the Massachusetts Institute of Technology, Research Laboratory of Electronics, jointly by the U.S. Army (Signal Corps), the U.S. Navy (Office of Naval Research), and the U.S. Air Force (Office of Scientific Research, Air Research and Development Command), under Signal Corps Contract DA36-039-sc-78108, Department of the Army Task 3-99-20-001 and Project 3-99-00-000, and was performed under Office of Naval Research Contract Nonr-1841(51).

MASSACHUSETTS INSTITUTE OF TECHNOLOGY

RESEARCH LABORATORY OF ELECTRONICS

Technical Report 377 January 15, 1961

# ANISOTROPY OF THERMOELECTRIC POWER IN BISMUTH TELLURIDE

Jane Hodgson Dennis

This report is identical with a thesis submitted to the Department of Electrical Engineering, M. I. T., in partial fulfillment of the requirements for the degree of Doctor of Philosophy.

## Abstract

Bismuth Telluride ($Bi_2Te_3$) has a hexagonal close-packed structure and highly anisotropic electrical and thermal conductivity. However, its thermoelectric-power tensor is only anisotropic under two rather special conditions. It is shown theoretically, on the basis of transport theory for the many-valleyed model of the band structure of $Bi_2Te_3$, that one way in which the thermoelectric power of this material can be made anisotropic is by causing two scattering mechanisms (lattice and impurity) to operate simultaneously in the material. Iodine-doped n-type material accordingly exhibits an anisotropy of thermoelectric power which is believed to be caused by this mixed scattering, whereas undoped p-type $Bi_2Te_3$ is found to have isotropic thermoelectric power for any temperature up to room temperature.

The theory also predicts that the thermoelectric power can be made anisotropic if there is simultaneous conduction by holes and electrons. Thus, above room temperature, when intrinsic conduction is setting in, the thermoelectric power of undoped p-type material indeed becomes anisotropic.

Single crystals of $Bi_2Te_3$ were grown in a crystal puller, and were used to make the necessary measurements of conductivity and thermoelectric power, in both crystallographic directions, over a wide range of temperature. These results of the measurements were in agreement with the predictions of the theory.

TABLE OF CONTENTS

CONTENTS

# CHAPTER I

## INTRODUCTION

At the time when the present study was undertaken, late in 1958, the occurrence of anisotropy of thermoelectric power was somewhat of a puzzle. There was certainly, at that time, no sound theoretical treatment of the origin of such anisotropy, although there were published reports of early (Boydston 1927) experimental data on the semimetal bismuth, and later reports (Goldsmid 1957) of observations of this effect in the semiconductor $Bi_2Te_3$. Goldsmid gave a crude explanation of the effect in iodine-doped n-type $Bi_2Te_3$, using isotropic models, which we shall describe.

The materials in which this effect has been observed have all been crystals of hexagonal (or rhombohedral) symmetry. A summary of all crystal symmetries in which this effect might be observed has been made (Nye 1957). Two of the principal crystallographic axes in these materials are equivalent for terms of first order in E, $\nabla T$, and H in the perturbation of the equilibrium distribution function. These two equivalent principal directions (in the based plane) can be distinguished by magnetoresistance and similar higher-order effects.

The electrical and thermal conductivity of the materials is generally highly anisotropic. It turns out, however, that the thermoelectric power is only anisotropic under certain rather special conditions that will be taken up in this work.

Bismuth is an intrinsic semimetal and thus has overlapping conduction and valence bands. It is therefore a two-carrier system. The anisotropy of thermoelectric power arises in such a system when the ratio of the mobility of holes to that of electrons is different in the two nonequivalent principal crystallographic directions. The detailed calculation has been carried out independently here and by Chandrasekhar (1959).

The semiconductor $Bi_2Te_3$ has two kinds of behavior which depend on the range of temperature considered and the level of doping. Above room temperature it becomes a two-carrier system and exhibits anisotropy of thermoelectric power for the same reason that bismuth does.

Below room temperature $Bi_2Te_3$ is usually a one-carrier system. Because the maximum of the liquidus solidus curve is on the bismuth-rich side of stoichiometry, undoped $Bi_2Te_3$ is p-type. It can become n-type by doping with sufficient iodine. The anisotropy of thermoelectric power arises in iodine-doped n-type $Bi_2Te_3$ because there are two scattering processes, lattice and impurity, operating at once. This results in a relaxation-time tensor from which the energy dependence is not factorable. In undoped p-type material only one scattering process (lattice) operates and hence the thermoelectric power is isotropic.

Goldsmid observed that the thermoelectric power was anisotropic in iodine-doped n-type $Bi_2Te_3$, but isotropic in undoped p-type material. He made a crude theoretical calculation, for a one-carrier system, based upon the following reasoning. He observed

that the thermoelectric power differed in the two nonequivalent principal crystallographic directions, as does the electrical conductivity. Then, using the parameters for one of the crystallographic directions, he imagines a homogeneous isotropic material with spherical energy surfaces, constructed in such a way that it has these same parameters. For this material, he works out the relationship between the thermoelectric power and the electrical conductivity. He then does this same thing for a homogeneous model having the parameters of the other crystallographic direction. He derives a relationship between the difference of the thermoelectric powers in the two principal crystallographic directions and the ratio of electrical conductivities in the two directions. He finds that this relationship is confirmed by experiment on $Bi_2Te_3$.

In this study we improve upon Goldsmid's work by analyzing carefully the more general anisotropic many-valleyed model of $Bi_2Te_3$. The relationship between thermoelectric power and electrical conductivity which he derived is found to be true for the more general model, provided that the electron statistics are classical. We also confirm his experimental result.

Thus it has been possible to observe in single crystals of essentially one material, $Bi_2Te_3$, anisotropy of thermoelectric power from two different internal mechanisms.

In Chapter II the theory of thermoelectric power is developed by using the anisotropic many-valleyed model for the electronic constant-energy surfaces that was used by Drabble (1956) to explain magnetoresistance in bismuth telluride. In the first part of Chaper II the tensor relationship between the flux of particles and the gradients of temperature and chemical potential for a one-carrier system is obtained. The thermoelectric power for a one-carrier system is then obtained from these tensors and the conditions for anisotropy are deduced. It was found that in order for the thermoelectric power to be anisotropic in such a system, the energy dependence of the relaxation-time tensor must not be factorable from it. It is shown that with the exponential type of scattering approximation normally used to make analysis tractable the only way to obtain this anisotropy condition is to have two competing scattering mechanisms, one of which (lattice scattering) is anisotropic. The relationship between the conductivity ratios and the difference between the thermoelectric powers for the two principal crystallographic directions of the material is then shown to hold for the general model, if the situation permits the use of classical statistics.

In the second part of Chapter II we consider a two-carrier system and find for it the tensor relationship between the current density and the gradients of temperature and chemical potential. The thermoelectric-power tensor is then found from these relationships and the conditions for anisotropy of thermoelectric power are determined without assuming a multiple-scattering mechanism. This anisotropy exists because the shape and orientation of the constant-energy surfaces for the conduction band are different from those for the valence band. The anisotropy condition can be expressed in terms of the mobility ratios in the principal directions, and becomes identical in form to the one used by Chandrasekhar for bismuth (although the details of the band structure

for the two materials are different.) (Our analysis was made independently of Chandrasekhar's.)

The preparation of the pulled single crystals of $Bi_2Te_3$ used in this work is described in Chapter III, and the method of cutting them is discussed.

Equipment for measuring the electrical conductivity of thermoelectric power and Hall effect is discussed, and the resulting data are presented in Chapter IV. We have measured the thermoelectric power at temperatures ranging from 100°K to 700°K for stoichiometric $Bi_2Te_3$ in both orientations, and for iodine-doped n-type $Bi_2Te_3$ in the temperature range 100°K-390°K also in both orientations. Electrical conductivity for both orientations of both types of material has been measured from 77°K to 310°K. The Hall effect of both materials has been measured only at room temperature and in one orientation.

In the first part of Chapter V the validity of the theory of thermoelectric power based upon mixed conduction and a single-scattering mechanism is checked on $Bi_2Te_3$ at high temperatures, at which the assumptions of the model are met. The agreement of theory with experiment is quite good.

In the second part of Chapter V the validity of the theory of thermoelectric power based on one-carrier conduction and a mixed scattering mechanism is discussed. The observed behavior with temperature of the anisotropy of thermoelectric power for $Bi_2Te_3$ is shown to agree qualitatively with the theory, and the predicted quantitative relationship between the conductivity ratios and the difference between the thermoelectric powers is shown to hold quite closely.

All of the experiments discussed here were carried out on pulled single crystals of $Bi_2Te_3$, which, to our knowledge, have not been studied before in the same context. The results are in agreement not only with the general theory but also with such other experimental data as are available on single-crystal material produced by different methods.

# CHAPTER II

## THEORY OF ANISOTROPY OF THERMOELECTRIC POWER

### 2.0 INTRODUCTION

Bismuth telluride is an anisotropic crystal of hexagonal close-packed ($\bar{3}$m) structure. Because of this anisotropy the simplest models of the constant-energy surfaces will not explain its transport properties. For example, a spherical energy surface gives purely isotropic results. A single ellipsoid of revolution will give anisotropic conductivity and Hall constant, but will predict that some magnetoresistance constants, which experience shows are appreciable, equal zero.

The model that we shall use for the energy-band structure of $Bi_2Te_3$ is that proposed by Drabble and Wolfe (1956) and used successfully by them to interpret magnetoresistance data in $Bi_2Te_3$. It consists of six ellipsoidal valleys centered in the reflection planes. The y-axis of the particular valley centered at $(K_x,0,K_z)$ is in the direction of the y-axis of the reciprocal lattice. The other valley axes are obtained from this one and by rotations that conform to crystal symmetry. Of course, the arrangement of the valleys satisfies the $\bar{3}$m symmetry of the crystal. See Fig. 2.1.

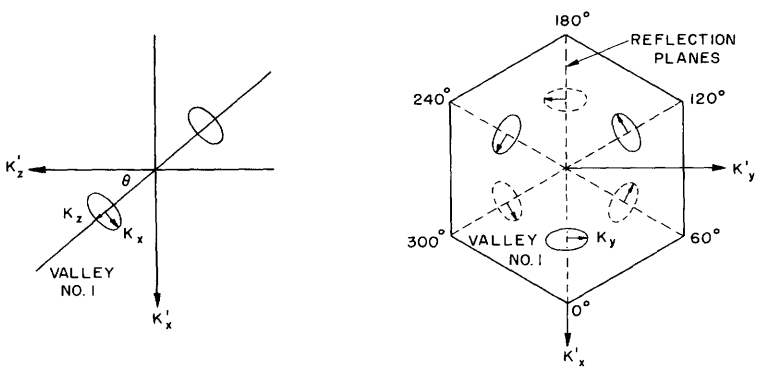


Fig. 2.1. Constant-energy surfaces.

We shall use the Boltzmann equation to find the perturbation of the equilibrium distribution function resulting from electrical and thermal gradients which we shall then use to find the transport equations for a single valley. The effects of all of the valleys will then be summed to obtain the transport equations for the entire crystal.

The thermoelectric power for the one-carrier case is computed from the coefficients of these equations. The assumptions concerning the relaxation time necessary to obtain anisotropy of thermoelectric power are discussed. A relationship between the ratio of conductivities along the cleavage planes and perpendicular to the planes and the difference between the thermoelectric power with heat flow in these directions is derived.

An expression for total current arising from both holes and electrons is obtained, and the thermoelectric power of the mixed conduction system is derived from this expression. The conditions on the forms of the constant-energy surfaces for the two carriers to obtain anisotropy of thermoelectric power are discussed. The expression for thermoelectric power is then put into a convenient form for computation.

## 2.1 DERIVATION OF TRANSPORT EQUATIONS

### 2.11 Transport Equations for a Single Valley

The Boltzmann equation is the equation of continuity in phase space. It represents the balance between the ordering forces (electrical and thermal gradients) and the disordering forces (collisions) in determining the distribution function. In the steady state the Boltzmann equation (Wilson 1953) is

$$\dot{r} \cdot \nabla_r f + \dot{p} \cdot \nabla_p f = \left.\frac{\partial f}{\partial t}\right|_{coll}$$

where $f$ is the distribution function of the particles; $\nabla_r$ is the gradient with respect to space; $\nabla_p$ is the gradient with respect to momentum; $\dot{p}$ is the acceleration of a particle between collisions; $\dot{r}$ is the velocity of the particle between collisions; and $\left.\frac{\partial f}{\partial t}\right|_{coll}$ is the time rate of change of the distribution function caused by collisions.

If the constant-energy surfaces in momentum space are assumed to be ellipsoids, the energy, $\underline{\underline{E}}$, is given by

$$\underline{\underline{E}} = \frac{1}{2}\,\vec{p} \cdot \left(\overleftrightarrow{\frac{1}{m}}\right) \cdot \vec{p}$$

where

$$\left(\overleftrightarrow{\frac{1}{m}}\right) = \begin{bmatrix} \frac{1}{m_1} & 0 & 0 \\ 0 & \frac{1}{m_2} & 0 \\ 0 & 0 & \frac{1}{m_3} \end{bmatrix}$$

when the coordinate axes are taken along the principal axes of the ellipsoid that is considered.

If the external fields perturb the distribution function only slightly from its equilibrium value, $f$ may be written (Bullis 1956)

$$f = f_o - \vec{G} \cdot \nabla_{\underline{\underline{p}}} \underline{\underline{E}} \frac{\partial f_o}{\partial \underline{\underline{E}}} + \cdots$$

where $f_o = \dfrac{1}{1 + \exp[(\underline{\underline{E}} - \epsilon)/kT]}$ is the equilibrium distribution function; $\vec{G}$ is a function of

the energy only; and $\nabla_{\underline{\underline{p}}}\underline{\underline{E}}$ is the group velocity of the particles. Bullis has shown that this is equivalent to expanding the distribution function in spherical harmonics.

The existence of a tensor relaxation time defined by

$$\left.\frac{df}{dt}\right|_{coll} = \left(\frac{\overleftrightarrow{1}}{\tau}\cdot\vec{G}\right)\cdot\nabla_{\underline{\underline{p}}}\underline{\underline{E}}\,\frac{\partial f_o}{\partial\underline{\underline{E}}}$$

where

$$\overleftrightarrow{\tau} = \begin{bmatrix}\tau_1 & 0 & 0\\ 0 & \tau_2 & 0\\ 0 & 0 & \tau_3\end{bmatrix}$$

is assumed. It is taken to be diagonal in the same axes as the effective mass tensor. If an electric field $\vec{E}$ and a thermal gradient $\nabla T$ are applied to the medium, $\dot{p} = q\vec{E}$ and $\dot{r} = \nabla_p E$, and the transport equation may be written

$$\nabla_{\underline{\underline{p}}}\underline{\underline{E}}\cdot\nabla_r\left[f_o - \vec{G}\cdot\nabla_{\underline{\underline{p}}}\underline{\underline{E}}\,\frac{df_o}{d\underline{\underline{E}}}\right] + q\vec{E}\cdot\nabla_p\left[f_o - \vec{G}\cdot\nabla_{\underline{\underline{p}}}\underline{\underline{E}}\,\frac{\partial f_o}{\partial\underline{\underline{E}}}\right] = \frac{\overleftrightarrow{1}}{\tau}\cdot\vec{G}\cdot\nabla_{\underline{\underline{p}}}\underline{\underline{E}}\,\frac{df_o}{d\underline{\underline{E}}}$$

Neglecting $\vec{G}\cdot\nabla_{\underline{\underline{p}}}\underline{\underline{E}}\,\frac{df_o}{d\underline{\underline{E}}}$ in the sums on the left-hand side but not in the product on the right-hand side, we have

$$\nabla_{\underline{\underline{p}}}\underline{\underline{E}}\cdot\nabla_r f_o + q\vec{E}\cdot\nabla_p f_o = \frac{\overleftrightarrow{1}}{\tau}\cdot\vec{G}\cdot\nabla_{\underline{\underline{p}}}\underline{\underline{E}}\,\frac{df_o}{d\underline{\underline{E}}}$$

The thermal gradient appears in $\nabla_r f_o$ because $f_o$ is a function of T. Thus

$$f_o(p, r) = \frac{1}{1 + \exp\left[\dfrac{\underline{\underline{E}}(p) - G(r)}{kT(r)}\right]} = \frac{1}{1 + e^{\alpha}}$$

where $\alpha = (\underline{\underline{E}}-\epsilon)/(kT)$, and it should be noted that $\epsilon$ is an implicit function of T. Thus

$$\nabla_r f_o = \frac{\partial f_o}{\partial\underline{\underline{E}}}\,\frac{\partial\underline{\underline{E}}}{\partial\alpha}\,\frac{\partial\alpha}{\partial T}\,\nabla_r T$$

and hence

$$\nabla_r f_o = -\frac{\partial f_o}{\partial\underline{\underline{E}}}\left[\frac{\underline{\underline{E}}}{T} + T\,\frac{d}{dT}\left(\frac{\epsilon}{T}\right)\right]\nabla_r T$$

Now

$$\nabla_p f_o = \nabla_{\underline{\underline{p}}}\underline{\underline{E}}\,\frac{df_o}{d\underline{\underline{E}}}$$

and so the transport equation becomes

$$-\nabla_{\underline{\underline{p}}}\underline{\underline{E}}\,\frac{df_o}{d\underline{\underline{E}}}\left[\frac{\underline{\underline{E}}}{T} + T\,\frac{d}{dT}\left(\frac{\epsilon}{T}\right)\right]\frac{dT}{dx} + q\vec{E}\cdot\nabla_{\underline{\underline{p}}}\underline{\underline{E}}\,\frac{df_o}{d\underline{\underline{E}}} = \frac{\overleftrightarrow{1}}{\tau}\cdot\vec{G}\cdot\nabla_{\underline{\underline{p}}}\underline{\underline{E}}\,\frac{\partial f_o}{\partial\underline{\underline{E}}}$$

The function $\nabla_{p\underline{\underline{E}}} \frac{\partial f_o}{\partial \underline{\underline{E}}}$ may be factored out, so that this equation may be solved for $\vec{G}$.

$$\vec{G} = -\left[\frac{\underline{\underline{E}}}{T} + T\frac{d}{dT}\left(\frac{\epsilon}{T}\right)\right]\overleftrightarrow{\tau} \cdot \nabla_r T + q\overleftrightarrow{\tau} \cdot \vec{E}$$

and the perturbed distribution function is, therefore,

$$f = f_o - \left(q\overleftrightarrow{\tau} \cdot \vec{E} - \left[\frac{\underline{\underline{E}}}{T} + T\frac{d}{dT}\left(\frac{\epsilon}{T}\right)\right]\overleftrightarrow{\tau} \cdot \nabla_r T\right) \cdot \nabla_{p\underline{\underline{E}}} \frac{df_o}{d\underline{\underline{E}}}$$

This function can now be used to find the fluxes of both particles and of heat. The flux of particles $\vec{J}^n_\nu$ resulting from valley $\nu$ alone is

$$\vec{J}^n_\nu = \frac{2}{h^3} \int_{\substack{\text{single} \\ \text{valley}}} \vec{\nabla}_p \underline{\underline{E}}\, f\, d^3p$$

and the flux of energy, $c_\nu$, carried by these particles is

$$\vec{C}_\nu = \frac{2}{h^3} \int_{\substack{\text{single} \\ \text{valley}}} \underline{\underline{E}}\, \nabla_p \underline{\underline{E}}\, f\, d^3p$$

All of the equations in this section are assumed to be in the coordinate system of a single valley. If the perturbed distribution function is inserted, an expression, which is appropriate for either the flux of particles or the flux of energy, is

$$\text{Flux}_\nu = -\frac{2}{h^3}\int\left(\underline{\underline{E}}^m \nabla_{p\underline{\underline{E}}}\left[q\overleftrightarrow{\tau} \cdot \vec{E} - \left[\frac{\underline{\underline{E}}}{T} + T\frac{d}{dT}\left(\frac{\epsilon}{T}\right)\right]\overleftrightarrow{\tau} \cdot \nabla T\right]\right) \cdot \nabla_{p\underline{\underline{E}}} \frac{df_o}{d\underline{\underline{E}}}\, d^3p$$

when m = 0 for particles $J^{(n)}$, and m = 1 for energy C.

Now assume the use of a mass tensor

$$\underline{\underline{E}} = \frac{p_1^2}{2m_1} + \frac{p_2^2}{2m_2} + \frac{p_3^2}{2m_3}$$

therefore

$$\nabla_{p\underline{\underline{E}}} = \frac{p_1}{m_1}\vec{i} + \frac{p_2}{m_2}\vec{j} + \frac{p_3}{m_3}\vec{k}$$

$$\overleftrightarrow{\tau} \cdot \vec{E} \cdot \nabla_{p\underline{\underline{E}}} = \frac{\tau_1 E_1 p_1}{m_1} + \frac{\tau_2 E_2 p_2}{m_2} + \frac{\tau_3 E_3 p_3}{m_3}$$

and

$$\tau \cdot \nabla T \cdot \nabla_{p\underline{\underline{E}}} = \tau_1 \frac{dT}{dx}\frac{p_1}{m_1} + \tau_2 \frac{dT}{dy}\frac{p_2}{m_2} + \tau_3 \frac{dT}{dz}\frac{p_3}{m_3}$$

Therefore the flux equation becomes

$$\text{Flux}_\nu = \frac{2}{h^3}\int \left(\frac{p_1}{m_1}\vec{i} + \frac{p_2}{m_2}\vec{j} + \frac{p_3}{m_3}\vec{k}\right)\left[q\left(\frac{\tau_1 E_1 p_1}{m_1} + \frac{\tau_2 E_2 p_2}{m_2} + \frac{\tau_3 E_3 p_3}{m_3}\right) - \left[\frac{\underline{\underline{E}}}{T} - T\frac{d}{dT}\left(\frac{\epsilon}{T}\right)\right]\left(\tau_1\frac{dT}{dx}\frac{p_1}{m_1} + \tau_2\frac{dT}{dy}\frac{p_2}{m_2} + \tau_3\frac{dT}{dz}\frac{p_3}{m_3}\right)\right]\underline{\underline{E}}^m \frac{df_o}{d\underline{\underline{E}}}\frac{ds_p}{\frac{\partial \underline{\underline{E}}}{\partial n_p}}d\underline{\underline{E}}$$

Here the integration was done first over a surface of constant energy and then with respect to the energy. From Bullis (1956) we find that the integral over a constant-energy surface is given by

$$\Omega_{rs} = \int p_r p_s \frac{ds_p}{\frac{\partial \underline{\underline{E}}}{\partial n_p}} = (m_1 m_2 m_3 m_r m_s)^{1/2}\,\pi\delta_{rs}\underline{\underline{E}}^{3/2}\,\frac{(2)^{7/2}}{3}$$

in which $\delta_{rs}$ is the Kronecker delta. A typical component of flux is therefore expressible as

$$\text{Flux}_{\nu i} = -\frac{2}{h^3}\int \left(\frac{q\tau_i E_i}{m_i^2}p_i^2 - \left[\frac{\underline{\underline{E}}}{T} + T\frac{d}{dT}\left(\frac{\epsilon}{T}\right)\right]\tau_i\frac{dT}{dx_i}\frac{p_i^2}{m_i^2}\right)\underline{\underline{E}}^m\frac{df_o}{d\underline{\underline{E}}}\frac{ds_p}{\frac{\partial \underline{\underline{E}}}{\partial n_1}}d\underline{\underline{E}}$$

or

$$\text{Flux}_{\nu i} = -\frac{2}{h^3}\int_0^\infty \left[\frac{q\tau_i E_i}{m_i^2} - \left[\frac{\underline{\underline{E}}}{T} + T\frac{d}{dT}\left(\frac{\epsilon}{T}\right)\right]\frac{\tau_i}{m_i^2}\frac{dT}{dx_i}\right]\underline{\underline{E}}^m\frac{df_o}{d\underline{\underline{E}}}d\underline{\underline{E}}\int_{\text{surface}} p_i^2\frac{ds_p}{\frac{2\underline{\underline{E}}}{dn_p}}$$

or

$$\text{Flux}_{\nu i} = -\frac{2^{9/2}\pi}{3h^3}(m_1 m_2 m_3)^{1/2}\,m_i\int_0^\infty\left(\frac{q\tau_i E_i}{m_i^2} - \left[\frac{\underline{\underline{E}}}{T} + T\frac{d}{dT}\left(\frac{\epsilon}{T}\right)\right]\frac{\tau_i}{m_i^2}\frac{dT}{dx_i}\right)\underline{\underline{E}}^{m+3/2}\frac{df_o}{d\underline{\underline{E}}}d\underline{\underline{E}}$$

Next let

$$K_j = \int \tau_i \underline{\underline{E}}^{j+1/2}\frac{df_o}{d\underline{\underline{E}}}d\underline{\underline{E}} \qquad (2.1\text{-}1)$$

and $\mathbf{E}$ be the gradient of a potential, $\phi$

$$\overline{E_i} = -\frac{d\phi}{dx_i}$$

We now have the two transport equations

$$J_{\nu i}^{(n)} = \frac{2^{9/2}}{3h^3}\frac{(m_1 m_2 m_3)^{1/2}}{m_i}\left[\left[\frac{qd\phi}{dx_i} + T\frac{d}{dT}\left(\frac{\epsilon}{T}\right)\frac{dT}{dx_i}\right]K_1 + \frac{1}{T}\frac{dT}{dx}K_2\right] \qquad (2.1\text{-}2)$$

and

$$C_{\nu i} = \frac{2^{9/2}}{3h^3}\frac{(m_1 m_2 m_3)^{1/2}}{m_i}\left[\left[\frac{qd\phi}{dx_i} + T\frac{d}{dT}\left(\frac{\epsilon}{T}\right)\frac{dT}{dx_i}\right]K_2 + \frac{1}{T}\frac{dT}{dx_i}K_3\right] \qquad (2.1\text{-}3)$$

These equations are inconvenient to transform because of the $\nabla(\epsilon/T)$ term. If we rearrange the first equation, multiply it by $\epsilon$, and subtract it from the second equation a more convenient form in which $\nabla(1/T)$ has been separated from $\nabla\epsilon$ will be achieved:

$$J_{\nu i}^{(n)} = \frac{2^{9/2}}{3h^3} \frac{(m_1 m_2 m_3)^{1/2}}{m_i} \left[ \frac{d}{dx_i} (\epsilon + e\phi) K_1 + (K_2 - \epsilon K_1) \frac{1}{T} \frac{dT}{dx_i} \right] \tag{2.1-4}$$

$$h_{\nu i} = \frac{2^{9/2}}{3h^3} \frac{(m_1 m_2 m_3)^{1/2}}{m_i} \left[ (K_2 - \epsilon K_1) \frac{d}{dx_i} (\epsilon + e\phi) \right] + \left[ K_3 - \epsilon K_2 \right] \frac{1}{T} \frac{dT}{dx_i} \tag{2.1-5}$$

Now $\bar{\mu} = (\epsilon + e\phi)$ is the electrochemical potential, and we have accordingly reduced the transport equations of a single valley to the form

$$J_{\nu i}^{(n)} = \alpha_i \frac{d\bar{\mu}}{dx_i} + \beta_i \frac{1}{T} \frac{dT}{dx_i} \tag{2.1-6}$$

$$h_{\nu i} = \beta_i \frac{d\bar{\mu}}{dx_i} + \gamma_i \frac{1}{T} \frac{dT}{dx_i} \tag{2.1-7}$$

where

$$\alpha_i = \frac{2^{9/2}\pi}{3h^3} \frac{(m_1 m_2 m_3)^{1/2}}{m_i} K_1 \tag{2.1-8}$$

$$\beta_i = \frac{2^{9/2}\pi}{3h^3} \frac{(m_1 m_2 m_3)^{1/2}}{m_i} (K_2 - \epsilon K_1) \tag{2.1-9}$$

and

$$\gamma_i = \frac{2^{9/2}\pi}{3h^3} \frac{(m_1 m_2 m_3)^{1/2}}{m_i} [K_3 - \epsilon K_2] \tag{2.1-10}$$

The equations given above represent the fluxes of particles and energy in a single valley, produced by forces applied along the principal axes of that valley. It is now necessary to consider how the effects of the six valleys add to produce the resulting transport equations for the whole crystal.

## 2.12 Transport Equations for the Whole Crystal

We must now transform each of the six sets of valley equations from the coordinate system of the individual valley to the coordinate system of the entire reciprocal lattice. We may then add the resulting equations to obtain the transport equations for the crystal as a whole.

It is convenient to make the transformation in two steps. The x'-axis lies in the

reflection plane of the valley and is parallel to the basal plane. The y'-axis is perpendicular to the reflection plane. First, xz-axes pertinent to a particular valley are rotated in the x-z plane, about the y-axis, in such a way that the valley z-axis coincides with the reciprocal lattice c-axis (z').

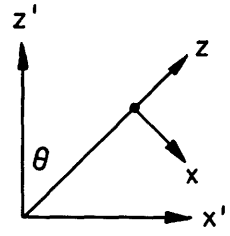


$$x = x' \cos\theta - z' \sin\theta$$

$$y = y'$$

$$z = x' \sin\theta + z' \cos\theta$$

These equations define a tensor

$$\boxed{x\ y\ z} = \overleftrightarrow{Q} \begin{bmatrix} x' \\ y' \\ z' \end{bmatrix}$$

where

$$\overleftrightarrow{Q} = \begin{bmatrix} c & 0 & -s \\ 0 & 1 & 0 \\ s & 0 & c \end{bmatrix}$$

when $c = \cos\theta$, and $s = \sin\theta$. Next, the resulting x'y'-axes are rotated about the z-axes to coincide with the lattice (the double prime) axes.

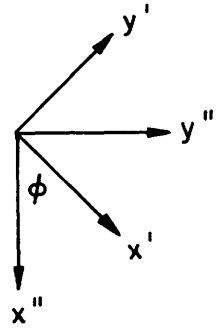


$$x' = x'' \cos\phi_\nu + y'' \sin\phi_\nu$$

$$y' = -x'' \sin\phi_\nu + y'' \sin\phi_\nu$$

$$z' = z$$

Here, $\phi = \nu\,(\pi/3)$, with $\nu = 1, 2, \ldots 6$. These equations define a tensor $\overleftrightarrow{T}_\nu$ that satisfies the expression

$$\boxed{x'\ y'\ z'} = \overleftrightarrow{T}_\nu \cdot \begin{bmatrix} x'' \\ y'' \\ z'' \end{bmatrix}$$

Let $a_\nu = \cos\phi_\nu$, $b_\nu = \sin\phi_\nu$, then

$$\overleftrightarrow{T}_\nu = \begin{bmatrix} a_\nu & b_\nu & 0 \\ -b_\nu & a_\nu & 0 \\ 0 & 0 & 1 \end{bmatrix} \qquad \nu = 1, 2, \ldots 6 \qquad (2.12\text{-}1)$$

There are six such tensors, one for each valley (each of which has a different value of $\nu$).

The expressions for the tensors $\overleftrightarrow{\alpha}$ and $\overleftrightarrow{\beta}$ in crystal space are, then,

$$\overleftrightarrow{\alpha}(c)_{\substack{\nu \\ \text{crystal} \\ \text{space}}} = \overleftrightarrow{T}_\nu^{-1}\,\overleftrightarrow{Q}^{-1}\,\overleftrightarrow{\alpha}(v)_{\substack{\text{valley} \\ \text{space}}}\,\overleftrightarrow{Q}\,\overleftrightarrow{T}_\nu$$

and

$$\beta(c)_{\substack{\nu \\ \text{crystal} \\ \text{space}}} = \overleftrightarrow{T}_\nu^{-1}\,\overleftrightarrow{Q}^{-1}\,\overleftrightarrow{\beta}(v)_{\substack{\text{valley} \\ \text{space}}}\,\overleftrightarrow{Q}\,\overleftrightarrow{T}_\nu$$

We have assumed that all the tensors that are of interest are diagonal in the valley axes. Then let

$$\overleftrightarrow{\alpha}(v) = \begin{bmatrix} \alpha_1 & & \\ & \alpha_2 & \\ & & \alpha_3 \end{bmatrix}$$

Now let us transform this tensor, which is diagonal in valley axes, into the reciprocal lattice axes.

$$\overleftrightarrow{\alpha}(v)Q = \begin{bmatrix} \alpha_1 c & \alpha_1 s & 0 \\ -\alpha_2 s & \alpha_2 c & 0 \\ 0 & 0 & \alpha_3 \end{bmatrix}$$

and

$$Q^{-1}\alpha(v)Q = \begin{bmatrix} \left(\alpha_1 c^2 + \alpha_2 s^2\right) & 0 & (\alpha_3 - \alpha_1)\,sc \\ 0 & & \\ (\alpha_3 - \alpha_1)\,sc & 0 & \left(\alpha_1 s^2 + \alpha_3 c^2\right) \end{bmatrix}$$

Hence

$$(Q^{-1}\alpha^{v}Q)\,T = \begin{bmatrix} a_\nu\left(\alpha_1 c^2 + \alpha_3 s^2\right) & b_\nu\left(\alpha_1 c^2 + \alpha_3 s^2\right) & (\alpha_3 - \alpha_1)\,sc \\ -b_\nu \alpha_2 & a_\nu \alpha_2 & 0 \\ a_\nu(\alpha_3 - \alpha_1)\,sc & b_\nu(\alpha_3 - \alpha_1)\,sc & \left(\alpha_1 s^2 + \alpha_3 c^2\right) \end{bmatrix}$$

and the tensor $\alpha$, diagonal in the axes of the valley $\nu$, is as transformed into the coordinates of the reciprocal lattice:

$$T^{-1}(Q^{-1}\alpha^{(\nu)}Q)\,T = \begin{bmatrix} \left[a_\nu^2\left(\alpha_1 c^2+\alpha_3 s^2\right)+b_\nu^2\alpha_2\right] & \left[a_\nu b_\nu\left(\alpha_1 c^2+\alpha_3 s^2\right)-a_\nu b_\nu \alpha_2\right] & \left[a_\nu(\alpha_3-\alpha_1)sc\right] \\ \left[a_\nu b_\nu\left(\alpha_1 c^2+\alpha_3 s^2\right)-a_\nu b_\nu \alpha_2\right] & \left[b_\nu^2\left(\alpha_1 c^2+\alpha_3 s^2\right)+a_\nu^2\alpha_2\right] & \left[b_\nu(\alpha_3-\alpha_1)sc\right] \\ \left[a_\nu(\alpha_3-\alpha_1)sc\right] & \left[b_\nu(\alpha_3-\alpha_1)sc\right] & \left[\alpha_1 s^2+\alpha_3 c^2\right] \end{bmatrix}$$

In order to obtain the total $\alpha$ tensor for the whole crystal (all six valleys), it is necessary to sum this tensor over all six values of $\nu$. The only elements of this tensor, which are different for different valleys, are the $a_\nu$ and $b_\nu$, and they are summarized in tabular form:

Valleys above z-axis

| Valley | $a_\nu$ | $b_\nu$ | $a_\nu b_\nu$ | $a_\nu^2$ | $b_\nu^2$ |
|---|---|---|---|---|---|
| 0 | 1 | 0 | 0 | 1 | 1 |
| 120° | $-\frac{1}{2}$ | $\frac{\sqrt{3}}{2}$ | $-\frac{\sqrt{3}}{4}$ | $\frac{1}{4}$ | $\frac{1}{4}$ |
| 240° | $-\frac{1}{2}$ | $-\frac{\sqrt{3}}{2}$ | $\frac{\sqrt{3}}{4}$ | $\frac{1}{4}$ | $\frac{1}{4}$ |
| Sum | 0 | 0 | 0 | 3 | 3 |

The resulting $\overleftrightarrow{\alpha}$ tensor for the whole crystal is therefore

$$\overleftrightarrow{\alpha}_{\text{crystal}} = \begin{bmatrix} 3\left(\alpha_1 c^2+\alpha_2+\alpha_3 s^2\right) & & \\ & 3\left(\alpha_1 c^2+\alpha_2+\alpha_3 s^2\right) & \\ & & 6\left(\alpha_1 s^2+\alpha_3 c^2\right) \end{bmatrix} \qquad (2.12\text{-}2)$$

Similarly, the $\beta$ tensor becomes

$$\overleftrightarrow{\beta}_{\text{crystal}} = \begin{bmatrix} 3\left(\beta_1 c^2+\beta_2+\beta_3 s^2\right) & & \\ & 3\left(\beta_1 c^2+\beta_2+\beta_3 s^2\right) & \\ & & 6\left(\beta_1 s^2+\beta_3 c^2\right) \end{bmatrix}$$

These $\overleftrightarrow{\alpha}$ and $\overleftrightarrow{\beta}$ tensors are diagonal because the x" and y" axes have been defined with respect to crystal symmetry to make them so.

## 2.2 THE THERMOELECTRIC POWER OF AN ANISOTROPIC CRYSTAL

The particle flux for the whole crystal is given by the tensor equation

$$\vec{J}^{(n)} = \overleftrightarrow{\alpha}\cdot\nabla_r\bar{\mu} + \frac{\overleftrightarrow{\beta}}{T}\cdot\nabla_r T \qquad (2.2\text{-}1)$$

If we insert $\bar{\mu} = \epsilon - e\phi$ in Eq. 2.2-1, we get

$$\vec{J}^{(n)} = \overleftrightarrow{a} \cdot (\nabla_r \epsilon - e\nabla_r \phi) + \frac{\overleftrightarrow{\beta}}{T} \cdot \nabla_r T \qquad (2.2\text{-}2)$$

This equation can be solved for

$$\nabla_r \phi = \frac{1}{e}\left[\nabla_r \epsilon - \overleftrightarrow{a}^{-1} \cdot \vec{J}^{(n)} + \frac{\overleftrightarrow{a}^{-1}}{T} \cdot (\beta \cdot \nabla_r T)\right.$$

The Seebeck voltage is defined as the potential difference across an open-circuited thermocouple (across points 1 and 2) as sketched in Fig. 2.2 with the two junctions between the materials A and B at two different temperatures, $T_1$ and $T_2$. Points 1 and 2 are at the same temperature. Mathematically, it is the integral of $\nabla\phi$ between points

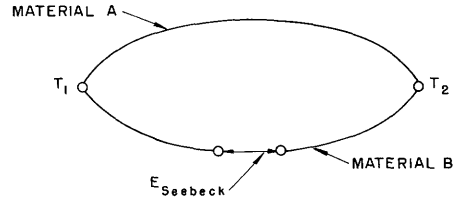


Fig. 2.2. A thermocouple.

1 and 2, with J = 0. Since $\nabla\phi$ is a scalar potential, this electromotive force is given by the integral of $\nabla\phi$ around the thermocouple wires from point 1 to point 2. We can then integrate Eq. 2.2-2 around the path with $J^{(n)}$ set equal to zero.

$$E_{Seebeck} = \frac{1}{e}\left[\int_1^2 \nabla_r \epsilon \cdot d\vec{r} + \int_{T_1}^{T_2} \left(\frac{\overleftrightarrow{a}^{-1}\overleftrightarrow{\beta}}{T}\right)_A \cdot \nabla_r T \cdot d\vec{r} + \int_{T_2}^{T_1} \left(\frac{\overleftrightarrow{a}^{-1}\overleftrightarrow{\beta}}{T}\right)_\beta \cdot \nabla_r T \cdot d\vec{r}\right]$$

$$= \frac{1}{e}\left[(\epsilon_2 - \epsilon_1) + \int_{T_1}^{T_2} \left(\frac{\overleftrightarrow{a}^{-1}\overleftrightarrow{\beta}}{T}\right)_A \cdot \nabla_r T \cdot d\vec{r} - \int_{T_1}^{T_2} \left(\frac{\overleftrightarrow{a}^{-1}\overleftrightarrow{\beta}}{T}\right)_\beta \cdot \nabla_r T \cdot d\vec{r}\right]$$

The Fermi level $\epsilon$ is a function of temperature only and will be the same at points 1 and 2, and so $(\epsilon_2 - \epsilon_1) = 0$.

Now the thermoelectric power of an individual material is defined as the limit of the Seebeck voltage per degree of temperature difference in the material as this temperature difference approaches zero. The thermoelectric power (TEP) is then given by

$$TEP = \frac{\overleftrightarrow{a}^{-1}\overleftrightarrow{\beta}}{eT} \qquad (2.2\text{-}3)$$

## 2.3 THERMOELECTRIC POWER PRODUCED BY ONE TYPE OF CHARGE CARRIER ONLY

The thermoelectric power tensor for the one-carrier case, from Eq. 2.2-3, is

$$\frac{a^{-1}\beta}{T} = \frac{1}{e}\begin{bmatrix} \dfrac{c^2\beta_1 + \beta_2 + s^2\beta_3}{c^2 a_1 + a_2 + s^2 a_3} & & \\ & \dfrac{c^2\beta_1 + \beta_2 + s^2\beta_3}{c^2 a_1 + a_2 + s^2 a_3} & \\ & & \dfrac{s^2\beta_1 + c^2\beta_3}{s^2 a_1 + c^2 a_3} \end{bmatrix} \qquad (2.3\text{-}1)$$

The 11 and 22 terms are equal, but the 33 term might be different. The 33 term will be different from the other two if any of the following conditions hold:

$$\frac{\beta_1}{a_1} \neq \frac{\beta_3}{a_3} \qquad \frac{\beta_1}{a_1} \neq \frac{\beta_2}{a_2} \qquad \frac{\beta_3}{a_3} \neq \frac{\beta_2}{a_2}$$

These inequalities in terms of the K integrals in Eq. 2.1-1 are equivalent to

$$K_1^x K_2^y \neq K_1^y K_2^x$$

$$K_1^y K_2^z \neq K_1^3 K_2^y$$

$$K_1^x K_2^z \neq K_1^z K_2^x$$

where x, y, and z refer to the component of the relaxation-time tensor that appears in the integral. Written out, these relations become

$$\int \tau_x \underline{\underline{E}}^{3/2} \frac{df_o}{d\underline{\underline{E}}} \int \tau_y \underline{\underline{E}}^{5/2} \frac{df_o}{d\underline{\underline{E}}} d\underline{\underline{E}} \neq \int \tau_y \underline{\underline{E}}^{3/2} \frac{df_o}{d\underline{\underline{E}}} d\underline{\underline{E}} \int \tau_x \underline{\underline{E}}^{5/2} \frac{df_o}{d\underline{\underline{E}}} d\underline{\underline{E}} \qquad (2.3\text{-}2)$$

Similarly, expressions can be written involving $\tau_x$ and $\tau_z$ and $\tau_y$ and $\tau_z$. It is easily seen that if $\tau_x = c_x \cdot f(\underline{\underline{E}})$, then the equality sign holds in these expressions.

Thus $\tau_x$ and $\tau_y$, $\tau_x$ and $\tau_z$, or $\tau_y$ and $\tau_z$ must be different functions of energy if these expressions are to be unequal. This means that the energy dependence of the relaxation-time tensor must not be factorable from the tensor itself.

There is no single scattering mechanism of the simple form usually used (energy to a power) that gives a nonfactorable energy dependence of the relaxation-time tensor. Such a tensor may be obtained by postulating the existence of two scattering mechanisms operating at once. One must be anisotropic, but the other may be isotropic. For

example, consider lattice scattering, which has a relaxation time of the form (Shockley 1950)

$$\tau_x^{\ell} = a\underline{\underline{E}}^{-1/2}$$

$$\tau_y^{\ell} = b\underline{\underline{E}}^{-1/2}$$

and impurity scattering, which has a relaxation time of the form $\tau_x^i = \tau_y^i = ce^q$. The collision frequencies are assumed to add as reciprocals:

$$\frac{1}{\tau} = \frac{1}{T^{\ell}} + \frac{1}{T^i}$$

that, in turn, becomes

$$\frac{1}{\tau_x} = \frac{1}{a\underline{\underline{E}}^{-1/2}} + \frac{1}{ce^q} = \frac{c\underline{\underline{E}}^q + a\underline{\underline{E}}^{-1/2}}{ac\underline{\underline{E}}^{-1/2+q}}$$

$$\frac{1}{\tau_y} = \frac{1}{be^{-1/2}} + \frac{1}{ce^q} = \frac{c\underline{\underline{E}}^q + b\underline{\underline{E}}^{-1/2}}{bc\underline{\underline{E}}^{-1/2+q}}$$

and so condition 2.3-2 becomes

$$\int \frac{ac\underline{\underline{E}}^{-1/2+q}}{c\underline{\underline{E}}^q + a\underline{\underline{E}}^{-1/2}} \underline{\underline{E}}^{3/2} \int \frac{bc\underline{\underline{E}}^{-1/2+q}}{ce^q + b\underline{\underline{E}}^{-1/2}} \underline{\underline{E}}^{5/2} \frac{df_o}{d\underline{\underline{E}}} d\underline{\underline{E}} \neq \int \frac{bc\underline{\underline{E}}^{-1/2+q}}{c\underline{\underline{E}}^q + b\underline{\underline{E}}^{-1/2}} \underline{\underline{E}}^{3/2} \frac{df_o}{d\underline{\underline{E}}} d\underline{\underline{E}}$$

$$\int \frac{ac\underline{\underline{E}}^{-1/2+q}}{c\underline{\underline{E}}^q + a\underline{\underline{E}}^{-1/2}} \underline{\underline{E}}^{5/2} \frac{df_o}{d\underline{\underline{E}}} d\underline{\underline{E}}$$

which can be simplified as

$$\int \frac{\underline{\underline{E}}}{1 + \frac{a}{c}\underline{\underline{E}}^{-(1/2+q)}} \frac{df_o}{d\underline{\underline{E}}} d\underline{\underline{E}} \int \frac{\underline{\underline{E}}^2}{1 + \frac{b}{c}\underline{\underline{E}}^{-(1/2+q)}} \frac{df_o}{d\underline{\underline{E}}} d\underline{\underline{E}} \neq \int \frac{\underline{\underline{E}}}{1 + \frac{b}{c}\underline{\underline{E}}^{-(1/2+q)}} \frac{df_o}{d\underline{\underline{E}}} d\underline{\underline{E}}$$

$$\int \frac{\underline{\underline{E}}^2}{1 + \frac{a}{c}\underline{\underline{E}}^{-(1/2+q)}} \frac{df_o}{dE} d\underline{\underline{E}}$$

which, in turn, can be further simplified as

$$\int_x \int_y \frac{xy^2}{(1+\nu x^{-(q+1/2)})(1+\mu y^{-(q+1/2)})} \frac{df_o}{dx} \frac{df_o}{dy} dxdy \neq \int_x \int_y \frac{x^2 y}{(1+\nu x^{-(q+1/2)})(1+\mu y^{-(q+1/2)})} \frac{df_o}{dx} \frac{df_o}{dy} dxdy$$

The inequality sign will hold unless $\nu = \mu$ or $a = b$. Thus we have shown that the thermoelectric power will be anisotropic if lattice scattering is anisotropic and there is another form of scattering, which may be isotropic, in addition to it.

## 2.4 RELATIONSHIP BETWEEN ANISOTROPY OF THERMOELECTRIC POWER AND THE CONDUCTIVITY RATIO

Goldsmid (1957) obtains an empirical relationship between $TEP_{33} - TEP_{11}$ and $(\sigma_{33})/\sigma_{11}$ by applying a simple classical spherical energy-surface model separately to each direction of the material. His argument runs as follows: If the relaxation time is assumed to be of the form

$$\tau_{\parallel}(\underline{\underline{E}}) = \tau_{o_{\parallel}} \underline{\underline{E}}^{(p_1)/2} \qquad \tau_{\perp}(\underline{\underline{E}}) = \tau_{o_{\perp}} \underline{\underline{E}}^{(p_3)/2}$$

in which the subscripts $\parallel$ and $\perp$ apply to properties measured with current or heat flow parallel to or perpendicular to the cleavage planes, respectively, then, for classical statistics,

$$TEP_{\parallel} = \frac{k}{e}\left[\frac{5 + p_1}{2} - \eta\right] \qquad TEP_{\perp} = \frac{k}{e}\left[\frac{5 + p_3}{2} - \eta\right]$$

and

$$TEP_{\perp} - TEP_{\parallel} = \frac{k}{e}\left(\frac{p_3 - p_1}{2}\right)$$

Now

$$\frac{\sigma_3}{\sigma_1} = \frac{\tau_{03}(kT)^{(3+p_3)/2}\left(\frac{3 + p_3}{2}\right)! \, e^{\xi/kT}}{\tau_{01}(kT)^{(3+p_1)/2}\left(\frac{3 + p_1}{2}\right)! \, e^{\xi/kT}}$$

and

$$\log \frac{\sigma_3}{\sigma_1} = \left(\frac{p_3 - p_1}{2}\right) \log kT + \text{constant}$$

therefore

$$TEP_{\perp} - TEP_{\parallel} = \frac{k}{e} \frac{d\left(\log \frac{\sigma_3}{\sigma_1}\right)}{d(\log kT)}$$

We shall now show that this same relationship holds for the many-valleyed model classical statistics. In order to do this we must make some preliminary calculations.

First, we must evaluate the integral

$$K_j = \int \tau_j(\underline{\underline{E}}) \, \underline{\underline{E}}^{j+1/2} \frac{df_o}{d\underline{\underline{E}}} \, d\underline{\underline{E}} \qquad (2.4\text{-}1)$$

We assume that

$$\tau_i(\underline{\underline{E}}) = \tau_{oi}\underline{\underline{E}}^{p_i/2}$$

Inserting this in Eq. 2.4-1, we obtain

$$K_j = \tau_{oi}\int \underline{\underline{E}}^{[(p_i+1)/2]+j}\frac{df_o}{d\underline{\underline{E}}}d\underline{\underline{E}}$$

Second, we must find the relationship between this integral and the tabulated integrals

$$\int_0^\infty \frac{x^q}{1+e^{x-\eta}}dx$$

The Fermi function is given by

$$f_o = \frac{1}{1+e^{(\underline{\underline{E}}-\epsilon)/kT}}$$

Define

$$x = \frac{\xi}{kT} \text{ and } \eta = \frac{\epsilon}{kT}$$

Then,

$$\frac{df_o}{dx} = kT\frac{df_o}{d\underline{\underline{E}}}$$

and Eq. 2.1-1 becomes

$$K_{ji} = \tau_{oi}(kT)^{[(p_i+1)/2]+j}\int x^{[(p_i+1)/2]+j}\frac{df_o}{dx}dx \qquad (2.4\text{-}2)$$

Integrating by parts, we find that

$$\int_0^\infty x^q\frac{df_o}{dx}dx = -q\int_0^\infty x^{q-1}f_o dx \qquad (2.4\text{-}3)$$

Inserting Eq. 2.4-3 in Eq. 2.4-2 yields

$$K_{ji} = -\tau_{oi}(kT)^{[(p_i+1)/2]+j}\left(\frac{p_i+1}{2}+j\right)\int_0^\infty x^{[(p_i+1)/2]+j-1}f_o dx \qquad (2.4\text{-}4)$$

These $K_j$ integrals enter into the thermoelectric-power expression in the form $K_2 - \epsilon K_1$. For classical statistics, the integrals become $\Gamma$ functions and there exists a simple relationship between them which is expressed as

$$\Gamma(n+1) = n\Gamma(n)$$

and therefore

$$K_2 - \epsilon K_1 = \tau_{oi}(kT)^{(p_i+3)/2}\left(\frac{p_i+3}{2}\right)\Gamma\left(\frac{p_i+3}{2}\right)\left[\frac{p_i+5}{2}-\eta\right] \qquad (2.4\text{-}5)$$

Use of Eqs. 2.1-8, 2.1-9, and 2.3-1 gives the difference between the parallel and perpendicular thermoelectric powers:

$$TEP_{\parallel} - TEP_{\perp} = \frac{1}{e}\left[\frac{\frac{c^2}{m_1}(K_2-\epsilon K_1)_1 + \frac{1}{m_2}(K_2-\epsilon K_1)_2 + \frac{s^2}{m_3}(K_2-\epsilon K_1)_3}{\frac{c^2}{m_1}(K_1)_1 + \frac{(K_1)_2}{m_2} + \frac{s^2}{m_3}(K_1)_3} - \frac{\frac{s^2}{m_1}(K_2-\epsilon K_1)_1 + \frac{c^2}{m_3}(K_2-\epsilon K_1)_3}{\frac{s^2}{m_1}(K_1)_1 + \frac{c^2}{m_3}(K_1)_3}\right]$$

From Eq. 2.4-5, this equation becomes

$$TEP_{\parallel} - TEP_{\perp} = \frac{k}{e}\left[\frac{\frac{c^2}{m_1}(kT)^{(p_1+3)/2}\left(\frac{p_1+3}{2}\right)\Gamma\left(\frac{p_1+3}{2}\right)\left[\frac{p_1+5}{2}-\eta\right] + \frac{1}{m_2}(kT)^{(p_2+3)/2}\left(\frac{p_2+3}{2}\right)\Gamma\left(\frac{p_2+3}{2}\right)\left[\frac{p_2+5}{2}-\eta\right] + \frac{s^2}{m_3}(kT)^{(p_3+3)/2}\left(\frac{p_3+3}{2}\right)\Gamma\left(\frac{p_3+3}{2}\right)\left[\frac{p_3+5}{2}-\eta\right]}{\frac{c^2}{m_1}(kT)^{(p_1+3)/2}\left(\frac{p_1+3}{2}\right)\Gamma\left(\frac{p_1+3}{2}\right) + \frac{1}{m_2}(kT)^{(p_2+3)/2}\left(\frac{p_2+3}{2}\right)\Gamma\left(\frac{p_2+3}{2}\right) + \frac{s^2}{m_3}(kT)^{(p_3+3)/2}\left(\frac{p_3+3}{2}\right)\Gamma\left(\frac{p_3+3}{2}\right)} - \frac{\frac{s^2}{m_1}(kT)^{(p_1+3)/2}\left(\frac{p_1+3}{2}\right)\Gamma\left(\frac{p_1+3}{2}\right)\left[\frac{p_1+5}{2}-\eta\right] + \frac{c^2}{m_3}(kT)^{(p_3+3)/2}\left(\frac{p_3+3}{2}\right)\Gamma\left(\frac{p_3+3}{2}\right)\left[\frac{p_3+5}{2}-\eta\right]}{\frac{s^2}{m_1}(kT)^{(p_1+3)/2}\left(\frac{p_1+3}{2}\right)\Gamma\left(\frac{p_1+3}{2}\right) + \frac{c^2}{m_3}(kT)^{(p_3+3)/2}\Gamma\left(\frac{p_3+3}{2}\right)}\right] \qquad (2.4\text{-}6)$$

The denominator of the first term in Eq. 2.4-6 is just $\sigma_{11}$. If the expressions in the brackets equal 1, the numerator would be $\sigma_{11}$ also. A similar statement involving $\sigma_{33}$ applies to the second term. Hence that part of the expression in the brackets, which is the same in all brackets (that is, $5/2-\eta$), cancels. This leaves only the $p_i/2$ factor in the brackets. Hence each term in the numerator is equal to the corresponding term in the denominator multiplied by the factor $p_i/2$. The numerator is then the derivative of the denominator and the following relationship holds for classical statistics:

$$TEP_{\parallel} - TEP_{\perp} = \frac{kT}{e}\left(\frac{1}{\sigma_1}\frac{d\sigma_1}{dT} + \frac{1}{\sigma_3}\frac{d\sigma_3}{dT}\right)$$

which when rearranged becomes

$$TEP_{\parallel} - TEP_{\perp} = \frac{k}{e}\frac{d\ln\left(\frac{\sigma_3}{\sigma_1}\right)}{d(\ln kT)} \qquad (2.4\text{-}7)$$

## 2.5 ANISOTROPY OF THERMOELECTRIC POWER ATTRIBUTED TO MIXED CONDUCTION

The phenomenological equations that are component forms of Eq. 2.2-1 for the flux of each type of carrier, are:

$$J_{i\,\text{electrons}}^{(n)} = \frac{J_{ie}}{-e} = \alpha_{ie}\frac{d\bar{\mu}_e}{dx_i} + \beta_{ie}\frac{1}{T}\frac{dT}{dx_i}$$

$$J_{i\,\text{holes}}^{(n)} = \frac{J_{ih}}{+e} = \alpha_{ih}\frac{d\bar{\mu}_h}{dx_i} + \beta_{ih}\frac{1}{T}\frac{dT}{dx_i} \qquad (2.5\text{-}1)$$

where the $\alpha$'s and $\beta$'s refer to the whole crystal. The relationship between $\left.\frac{d\bar{\mu}}{dx_i}\right|_{\text{holes}}$ and $\left.\frac{d\bar{\mu}}{dx_i}\right|_{\text{electrons}}$ is found in the following way. The chemical potential for electrons is

$$\bar{\mu}_e = \epsilon_e - e\phi = E_f - E_c - e\phi$$

and for holes is

$$\bar{\mu}_h = \epsilon_h + e\phi = E_v - E_f + e\phi$$

Summing these two equations gives

$$\bar{\mu}_e + \bar{\mu}_h = E_v - E_c = -E_g$$

Differentiating this equation and assuming $E_g$ to be constant with position gives

$$\frac{d\bar{\mu}_e}{dx_i} = -\frac{d\bar{\mu}_h}{dx_i} \qquad (2.5\text{-}2)$$

If we insert Eq. 2.5-2 in Eqs. 2.5-1, the current produced by the electrons is given by

$$J_e = +e\alpha_{ie}\frac{d\bar{\mu}_h}{dx_i} - e\beta_{ie}\frac{1}{T}\frac{dT}{dx_i}$$

and the current produced by holes is given by

$$J_h = e\alpha_{ie}\frac{d\bar{\mu}_h}{dx_i} + e\beta_{ih}\frac{1}{T}\frac{dT}{dx_i}$$

The total current is given by

$$J_e + J_h = e(\alpha_{ih}+\alpha_{ie})\frac{d\bar{\mu}_h}{dx_i} + e(\beta_{ih}-\beta_{ie})\frac{1}{T}\frac{dT}{dx_i}$$

The $\alpha$-tensor for the two-carrier system is, then, the sum of the $\alpha$-tensors for the two one-carrier cases. The $\beta$-tensor is the difference of the tensors for the two cases.

Written in matrix form, the corresponding $\alpha$ and $\beta$ tensors are:

$$\overleftrightarrow{\alpha} = \begin{bmatrix} 3\left(\alpha_1 c^2+\alpha_2+\alpha_3 s^2\right)_e + 3\left(\alpha_1 c^2+\alpha_2+\alpha_3 s^2\right)_h & & \\ & 3\left(\alpha_1 c^2+\alpha_2+\alpha_3 s^2\right)_e + 3\left(\alpha_1 c^2+\alpha_2+\alpha_3 s^2\right)_h & \\ & & 6\left(\alpha_1 s^2+\alpha_3 c^2\right)_e + 6\left(\alpha_1 s^2+\alpha_3 c^2\right)_h \end{bmatrix}$$

$$\overleftrightarrow{\beta} = \begin{bmatrix} -3\left(\beta_1 c^2+\beta_2+\beta_3 s^2\right)_e + 3\left(\beta_1 c^2+\beta_2+\beta_3 s^2\right)_h & & \\ & -3\left(\beta_1 c^2+\beta_2+\beta_3 s^2\right)_e + 3\left(\beta_1 c^2+\beta_2+\beta_3 s^2\right)_h & \\ & & -6\left(\beta_1 s^2+\beta_3 c^2\right)_e + 6\left(\beta_1 s^2+\beta_3 c^2\right)_h \end{bmatrix}$$

(2.5-3)

and, from Eq. 2.2-2, the thermoelectric-power tensor is

$$\frac{\alpha^{-1}\beta}{eT} = \frac{1}{eT}\begin{bmatrix} \dfrac{-3\left(\beta_1 c^2+\beta_2+\beta_3 s^2\right)_e + 3\left(\beta_1 c^2+\beta_2+\beta_3 s^2\right)_h}{+3\left(\alpha_1 c^2+\alpha_2+\alpha_3 s^2\right)_e + 3\left(\alpha_1 c^2+\alpha_2+\alpha_3 s^2\right)_h} & & \\ & \dfrac{-3\left(\beta_1 c^2+\beta_2+\beta_3 s^2\right)_e + 3\left(\beta_1 c^2+\beta_2+\beta_3 s^2\right)_h}{+3\left(\alpha_1 c^2+\alpha_2+\alpha_3 s^2\right)_e + 3\left(\alpha_1 c^2+\alpha_2+\alpha_3 s^2\right)_h} & \\ & & \dfrac{-6\left(\beta_1 s^2+\beta_3 c^2\right)_e + 6\left(\beta_1 s^2+\beta_3 c^2\right)_h}{+6\left(\alpha_1 s^2+\alpha_3 c^2\right)_e + 6\left(\alpha_1 s^2+\alpha_3 c^2\right)_h} \end{bmatrix}$$

(2.5-4)

The tensors of the individual ellipsoids ($\nu$) in terms of fundamental physical quantities, from Eq. 2.1-8 and 2.1-9, are:

$$\alpha_{\nu ie} = \frac{2^{9/2}}{3}\pi\frac{(m_1 m_2 m_3)_e^{1/2}}{m_{ie}} m_o^{1/2}\int \tau_{ie}\underline{\underline{E}}^{3/2}\frac{df_o}{d\underline{\underline{E}}}d\underline{\underline{E}}$$

$$\beta_{\nu ie} = \frac{2^{9/2}}{3}\pi\frac{(m_1 m_2 m_3)_e^{1/2}}{m_{ie}} m_o^{1/2}\left[\int \tau_{ie}\underline{\underline{E}}^{5/2}\frac{df_o}{d\underline{\underline{E}}} - \frac{\underline{\underline{E}}}{kT}\int \tau_{i}\underline{\underline{E}}^{3/2}\frac{df_o}{d\underline{\underline{E}}}d\underline{\underline{E}}\right]$$

(2.5-5)

$$\alpha_{\nu ih} = \frac{2^{9/2}}{3}\pi\frac{(m_1 m_2 m_3)_h^{1/2}}{m_{ih}} m_o^{1/2}\int \tau_{ih}\underline{\underline{E}}^{3/2}\frac{df_o}{d\underline{\underline{E}}}d\underline{\underline{E}}$$

$$\beta_{\nu ih} = \frac{2^{9/2}}{3}\pi\frac{(m_1 m_2 m_3)_h^{1/2}}{m_{ih}} m_o^{1/2}\left[\int \tau_{ih}\underline{\underline{E}}^{5/2}\frac{df_o}{d\underline{\underline{E}}}d\underline{\underline{E}} - \frac{\epsilon}{kT}\int \tau_{ih}\underline{\underline{E}}^{3/2}\frac{df_o}{d\underline{\underline{E}}}d\underline{\underline{E}}\right]$$

Let us assume that lattice scattering for which $\tau_i = \tau_o \underline{\underline{E}}^{-1/2}$, with $\tau_o$ a function of temperature $\left(\sim \frac{1}{T}\right)$, is dominant. In order to evaluate the integrals in Eqs. 2.5-5, it is necessary to know the relationship

$$\int_0^\infty \underline{\underline{E}}^p \frac{df_o}{d\underline{\underline{E}}} \, d\underline{\underline{E}} = -p \int_0^\infty \underline{\underline{E}}^{p-1} f_o \, d\underline{\underline{E}} = -pF_{p-1}(\eta)$$

With the assumption $\tau_i = \tau_o \underline{\underline{E}}^{-1/2}$, Eqs. 2.5-4 take the following form:

$$\alpha_{\nu ie} = \frac{2^{7/2}}{3} \pi m_o^{1/2} \, kT \, \tau_{oe} \frac{(m_1 m_2 m_3)_e^{1/2}}{m_{ie}} F_o(\eta_e)$$

$$\beta_{\nu ie} = \frac{2^{7/2}}{3} \pi m_o^{1/2} (kT)^2 \, \tau_{oe} \frac{(m_1 m_2 m_3)_e^{1/2}}{m_{ie}} \left[2F_1(\eta_e) - \frac{\epsilon}{kT} F_o(\eta_e)\right] \tag{2.5-6}$$

$$\alpha_{\nu ih} = \frac{2^{7/2}}{3} \pi m_o^{1/2} \, kT \, \tau_{oh} \frac{(m_1 m_2 m_3)_h^{1/2}}{m_{ih}} F_o(\eta_h)$$

$$\beta_{\nu ih} = \frac{2^{7/2}}{3} \pi m_o^{1/2} (kT)^2 \, \tau_{oh} \frac{(m_1 m_2 m_3)_h^{1/2}}{m_{ih}} \left[2F_1(\eta_h) - \frac{\epsilon}{kT} F_o(\eta_h)\right]$$

Inserting Eq. 2.5-6 in Eq. 2.5-4, we obtain

$$\left(\frac{\alpha^{-1}\beta}{eT}\right)_{\parallel} = \left(\frac{\alpha^{-1}\beta}{eT}\right)_{\perp} = \frac{1}{e}\left[\frac{-k(m_1m_2m_3)_e^{1/2}\tau_{oe}\left(\frac{s^2}{m_1}+\frac{1}{m_2}+\frac{s^2}{m_3}\right)_e[2F_1(\eta_e)-\eta_e F_o(\eta_e)] + k(m_1m_2m_3)_h^{1/2}\tau_{oh}\left(\frac{s^2}{m_1}+\frac{1}{m_2}+\frac{s^2}{m_3}\right)_h[2F_1(\eta_h)-\eta_h F_o(\eta_h)]}{(m_1m_2m_3)_e^{1/2}\tau_{oe}\left(\frac{c^2}{m_1}+\frac{1}{m_2}+\frac{s^2}{m_3}\right)_e F_o(\eta_e) + (m_1m_2m_3)_h^{1/2}\tau_{oh}\left(\frac{c^2}{m_1}+\frac{1}{m_2}+\frac{s^2}{m_3}\right) F_o(\eta_h)}\right] \tag{2.5-7a}$$

We define

$$\delta_{\parallel} = \frac{\tau_{oh}(m_1m_2m_3)_h^{1/2}\left(\frac{c^2}{m_1}+\frac{1}{m_2}+\frac{s^2}{m_3}\right)_h}{\tau_{oe}(m_1m_2m_3)_e^{1/2}\left(\frac{c^2}{m_1}+\frac{1}{m_2}+\frac{s^2}{m_3}\right)_e} \tag{2.5-7b}$$

and Eq. 2.5-7a becomes

$$TEP_{11} = TEP_{22} = \frac{k}{e}\left[\frac{-[2F_1(\eta_e)-\eta_e F_o(\eta_e)] + \delta_{\parallel}[2F_1(\eta_h)-\eta_h F_o(\eta_h)]}{F_o(\eta_e) + \delta_{\parallel} F_o(\eta_h)}\right] \tag{2.5-7c}$$

Similarly, if we define

$$\delta_{\perp} = \frac{\tau_{oh}(m_1 m_2 m_3)_h^{1/2}\left(\frac{s^2}{m_1} + \frac{c^2}{m_3}\right)_h}{\tau_{oe}(m_1 m_2 m_3)_e^{1/2}\left(\frac{s^2}{m_1} + \frac{c^2}{m_3}\right)_e} \tag{2.5-7d}$$

then the component of thermoelectric power perpendicular to the cleavage plane becomes

$$TEP_{\perp} = \frac{k}{e}\left[\frac{-[2F_1(\eta_e) - \eta_e F_o(\eta_e)] + \delta_{\perp}[2F_1(\eta_h) - \eta_h F_o(\eta_h)]}{F_o(\eta_e) + \delta_{\perp} F_o(\eta_h)}\right] \tag{2.5-7e}$$

The thermoelectric power will be anisotropic only if

$$\left(\frac{\alpha^{-1}\beta}{eT}\right)_{\parallel} \neq \left(\frac{\alpha^{-1}\beta}{eT}\right)_{\perp}$$

This will be so if $\delta_{\parallel} \neq \delta_{\perp}$, which is equivalent to

$$\frac{\left(\frac{c^2}{m_1} + \frac{1}{m_2} + \frac{s^2}{m_3}\right)_h}{\left(\frac{c^2}{m_1} + \frac{1}{m_2} + \frac{s^2}{m_3}\right)_e} \neq \frac{\left(\frac{s^2}{m_1} + \frac{c^2}{m_3}\right)_h}{\left(\frac{s^2}{m_1} + \frac{c^2}{m_3}\right)_e} \tag{2.5-8}$$

In order for inequality 2.5-8 to become an equality, the valence and conduction-band models would either have to be identical, or they would have to be different in a very special way; that is, the ratios on the two sides of the equation would have to be equal. It seems unlikely that either condition would occur except, perhaps, by accident. It seems likely that the thermoelectric power would be anisotropic over any temperature range in which there is mixed conduction.

By considering the mobility ratio, the expressions for thermoelectric power (Eqs. 2.5-7) may be put into a more convenient form. To achieve this result, note first that by using Eqs. 2.5-5 and 2.12-1 the parallel resistivity can be written

$$\alpha_{11} = \sigma_{11} = \frac{2^{9/2}}{3}\pi m_o^{1/2}(kT)\,\tau_o(m_1 m_2 m_3)^{1/2}\left(\frac{c^2}{m_1} + \frac{1}{m_2} + \frac{s^2}{m_3}\right) F_o(\eta) \tag{2.5-9}$$

and the number of carriers is given by

$$n = 2^{9/2}\pi \frac{(m_1 m_2 m_3)^{1/2}}{h^3} m_o^{3/2}(kT)^{3/2}\, F_{1/2}(\eta) \tag{2.5-10}$$

Thus the mobility of electrons in the parallel direction is given by

$$\mu_e = \frac{\sigma}{\eta_e} = \frac{(kT)^{-1/2}}{m_o} h^3\, \tau_{oe}\left(\frac{c^2}{m_1} + \frac{1}{m_2} + \frac{s^2}{m_3}\right)_e \frac{F_o(\eta_e)}{F_{1/2}(\eta_e)}$$

and the mobility of holes is given by

$$\mu_h = \frac{(kT)^{-1/2}}{m_o} h^3 \tau_{oh} \left( \frac{c^2}{m_1} + \frac{1}{m_2} + \frac{s^2}{m_3} \right)_h \frac{F_o(\eta_h)}{F_o(\eta_e)}$$

The mobility ratio for the parallel direction, accordingly, is

$$\left. \frac{\mu_h}{\mu_e} \right|_{\parallel} = \frac{\tau_{oh} \left( \frac{c^2}{m_1} + \frac{1}{m_2} + \frac{s^2}{m_3} \right)_h \frac{F_o(\eta_h)}{F_{1/2}(\eta_h)}}{\tau_{oe} \left( \frac{c^2}{m_1} + \frac{1}{m_2} + \frac{s^2}{m_3} \right)_e \frac{F_o(\eta_e)}{F_{1/2}(\eta_e)}} \tag{2.5-11}$$

This expression may be used to find the thermoelectric power in terms of the mobility ratio, by inserting Eq. 2.5-11 in Eqs. 2.5-7.

$$TEP_{\parallel,\perp} = \frac{k}{e} \frac{-[2F_1(\eta_e) - \eta_e F_o(\eta_e)] + \left( \frac{m_h^*}{m_e^*} \right)^{3/2} \left( \frac{\mu_h}{\mu_e} \right)_{\parallel,\perp} \frac{F_o(\eta_e)}{F_{1/2}(\eta_e)} \frac{F_{1/2}(\eta_h)}{F_o(\eta_h)} [2F_1(\eta_h) - \eta_h F_o(\eta_h)]}{F_o(\eta_e) + \left( \frac{m_h^*}{m_e^*} \right)^{3/2} \left( \frac{\mu_h}{\mu_e} \right)_{\parallel,\perp} \frac{F_o(\eta_e)}{F_{1/2}(\eta_e)} \frac{F_{1/2}(\eta_h)}{F_o(\eta_h)} F_o(\eta_h)} \tag{2.5-12}$$

Define a convenient parameter $\gamma$ by the relations

$$\gamma_{\parallel} = \left( \frac{m_h^*}{m_e^*} \right)^{3/2} \left( \frac{\mu_h}{\mu_e} \right)_{\parallel}$$

and

$$\gamma_{\perp} = \left( \frac{m_h}{m_e} \right)^{3/2} \left( \frac{\mu_h}{\mu_e} \right)_{\perp}$$

Then Eq. 2.5-12 becomes

$$TEP_{\parallel,\perp} = \frac{k}{e} \frac{-\left[ \frac{2F_1(\eta_e) F_{1/2}(\eta_e)}{F_o(\eta_e)} - \eta_e F_{1/2}(\eta_e) \right] + \gamma_{\parallel,\perp} \left[ \frac{2F_1(\eta_h) F_{1/2}(\eta_h)}{F_o(\eta_h)} - \eta_h F_{1/2}(\eta_h) \right]}{F_{1/2}(\eta_e) + \gamma_{\parallel,\perp} F_{1/2}(\eta_h)} \tag{2.5-13}$$

The parameters of Eqs. 2.5-7 are functions only of the effective masses and the angles, and the form of the equation makes it convenient to assume that these are constant. One might think that these $\delta$'s would be more nearly constant with temperature

than the $\gamma$ parameters of Eq. 2.5-13 which are products of the $\delta$ factors and $\frac{F_o(\eta_e)}{F_{1/2}(\eta_e)} \frac{F_{1/2}(\eta_h)}{F_o(\eta_h)}$ (the Fermi product). This Fermi factor product decreases approximately 30 per cent from 77°K to room temperature.

We first computed the intrinsic thermoelectric power, using Eq. 2.5-7. We used the density-of-states effective masses, the mobility ratios, and the value of the Fermi level obtained from thermoelectric-power measurements at 77°K by Drabble et al. to compute the parameters at 77°K. We then assumed that the $\delta$'s remain constant and computed the intrinsic thermoelectric power from Eq. 2.5-7, using these $\delta$'s and the appropriate high-temperature Fermi functions. The agreement with experiment was poor — the values of thermoelectric power were too large. The intrinsic value of thermoelectric power, in the parallel orientation, computed in this way, was 90 $\mu$v/degree, against an experimental result of approximately 60 $\mu$v/degree.

On the other hand, when we assumed the mobility ratio, which is $\delta$ times the Fermi factor product, to be constant (at its value at 77°K obtained by Drabble et al.), and used Eq. 2.5-13 to compute the intrinsic thermoelectric power, the computed result agreed quite well with the experimental value of 60 $\mu$v/degree. Hence, we have concluded that the mobility ratio of this material is more nearly constant than the factors involving the effective masses and angles.

# CHAPTER III

# PREPARATION OF SINGLE CRYSTALS OF BISMUTH TELLURIDE

## 3.1 PROPERTIES AND STRUCTURE OF $Bi_2Te_3$

$Bi_2Te_3$ has a rhombohedral unit cell with $R\bar{3}m$ symmetry. There is one linear molecule per unit cell. (See Figs. 3.1-1 and 3.1-2.) The following list gives its crystallographic properties (Wyckoff 1948):

a = 10.47 A

$\alpha$ = 24°8'

1 Te at 0, 0, 0

2 Bi at ± u, u, u

2 Te at ± v, v, v

u = 0.399

v = 0.792

This material has very marked cleavage planes at right angles to the axis of the crystal. The cohesive force between these cleavage planes is so weak that the material splits

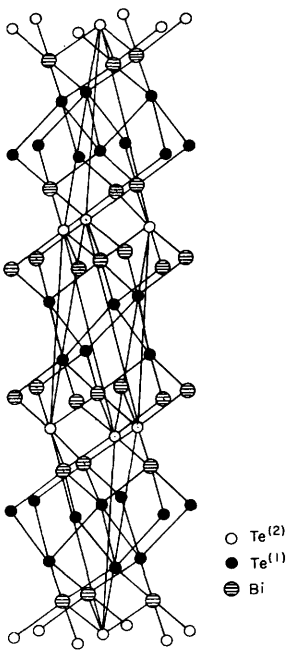


Fig. 3.1-1. Structure of $Bi_2Te_3$. (From Harker, Z. Krist. 33, 181, 1934.)

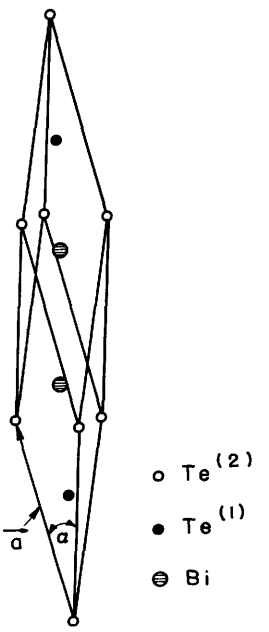


Fig. 3.1-2. Unit cell of $Bi_2Te_3$.

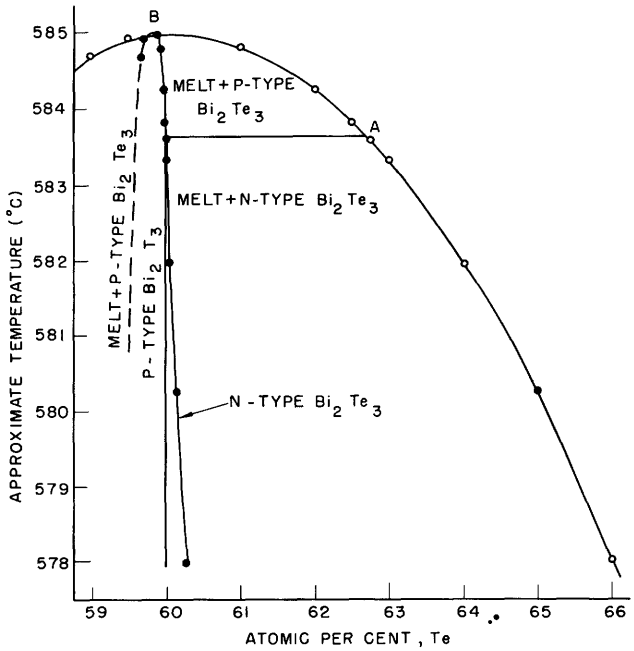


Fig. 3.1-3. Liquidus solidus curve of the bismuth-tellurium system. (From C. B. Satterthwaite and R. W. Ure, Jr., Phys. Rev. 108, 1165, 1957.)

very easily. The melting temperature is 585°C and the maximum in the liquidus solidus curve (Fig. 3.1-3) is on the bismuth-rich side of the stoichiometric composition (Satterthwaite and Ure 1957), and hence single undoped crystals are p-type.

## 3.2 PREPARATION OF SINGLE CRYSTALS OF BISMUTH TELLURIDE

Single crystals of both p-type and iodine-doped n-type $Bi_2Te_3$, of approximate dimensions 12 cm × 2 cm × 3 mm, have been grown in a Czochralski type of crystal-pulling apparatus. The material used for growing the crystals was semiconductor grade bismuth and tellurium of stated nominal purity of 99.999+ per cent obtained from the American Smelting and Refining Company. At first, this material was placed directly in the crucible and the reaction took place in the crystal puller. There was always a slag deposit on top of the melt, usually covering most of it. The reacted material was cooled, removed from the crucible, and the slag scraped off. After a second melting, the surface was usually visibly clean, although a little slag did accumulate on the coldest part of the edge of the melt.

Seeds would start fairly easily in this melt, and the growth had a strong tendency to thicken by forming step growths, which will be described in more detail in this section. A seed could be allowed to thicken, in this way, up to 2.9 mm, but when it was grown at this thickness for 1 or 2 inches, visible longitudinal pleats indicating gross imperfections appeared in the crystal. These pleats emanated from little nucleations on the surface of the crystal which would then pile on top of each other and result in a pleated surface. The tellurium for the melts was distilled three times thereafter. In melts made with distilled tellurium the crystals did not thicken readily, but the imperfections decreased as the growth progressed. The trick needed to obtain thick growths, then, is to let a

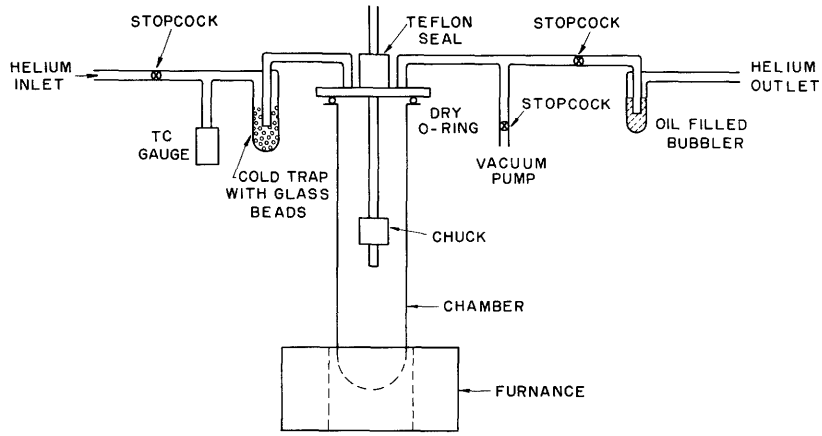


Fig. 3.2-1. Crystal puller.

small seed in an impure melt widen and thicken to the desired size, and then let this expanded seed continue the growth as long as desired in a purified melt.

The first crystals were grown in an apparatus previously developed in our laboratory. In spite of very careful cleaning of this equipment, the melts usually became dirty. Small amounts of vacuum grease on the apparatus heated by the furnace resulted in contamination of the melt. Because grease was used on the pushrod and chamber seals, it was very difficult to alleviate this problem.

A new apparatus, partially modeled after one used by Freeman D. Shepherd at the Air Force Cambridge Research Center, (Shepherd 1959) was developed. This apparatus had a dry O-Ring chamber seal and a Teflon pushrod seal. In it consistently clean melts were achieved. A sketch of the new apparatus is shown in Fig. 3.2-1. The second procedure for growing crystals is similar to that described by Shepherd (1959); The melt is placed in the crucible, the seed mounted in its holder, and the apparatus assembled. The apparatus is then pumped down to a good forepump vacuum (10 $\mu$). Helium is admitted to the chamber and the system is pumped down again. This helium flushing procedure, repeated several times, removes all of the oxygen from the system. Helium is then admitted with a slight over-pressure.

The furnace is raised to a position that is such that the melt is well down in it. The controller is set for a temperature above the melting point of $Bi_2Te_3$, but not so high that a yellow vapor of bismuth and tellurium appears. Otherwise, the vapor condenses on the seed, forming sites for nucleation of crystallites. The presence of these sites makes it difficult to stop growth of a polycrystal (even at growing temperature some condensation occurs, but it can be minimized by keeping the temperature as low as possible).

After the material is melted, it must be brought to proper growing temperature. The furnace is lowered so that the top of the melt is approximately 0.125 inch below the top of the furnace. The temperature at which the controller is set is lowered slowly, in a manner that keeps the system in thermal equilibrium (that is, in such a way that transient conditions are avoided and the set point actually determines the temperature) until the material just begins to solidify around the edge of

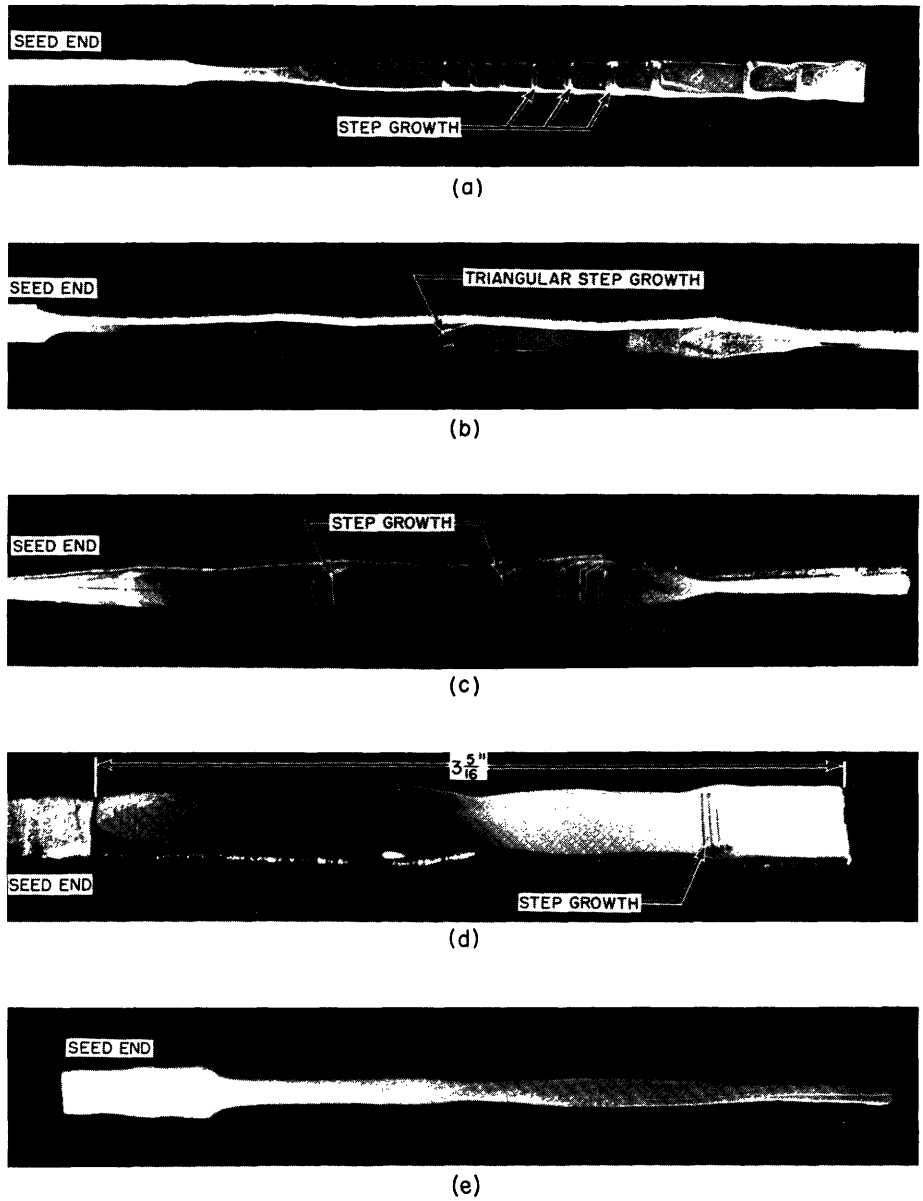


Fig. 3.2-2. Single crystals of bismuth telluride.

the crucible. The seed may then be lowered into the melt and fine adjustment of the temperature can be made.

The temperature is correct for pulling if the melt is just hot enough to form an upward-directed meniscus around the seed, but not so hot that the crystal necks down too rapidly or breaks off. Once the growth has been started successfully, the temperature may be lowered to widen and thicken the crystal.

As we have mentioned, thickening often occurs in steps (see Fig. 3.2-2a-d). A crystal grown at constant temperature, giving only slight evidence of step growth, is shown in Fig. 3.2-2e.

In order to maintain a uniform melt temperature, the seed with the growing crystal

was rotated to provide stirring action. In spite of this rotational motion, it is seen from Fig. 3.2-2 that a flat-shaped crystal resulted. The flat faces are the cleavage planes of the crystal. Thus the hexagonal c-axis is normal to these flat faces. The persistence of the flat shape of the crystal indicates a very high anisotropy in the energy of formation of the various crystal planes.

Since the volume of the crystal pulled per unit time is equal to the crystallization rate, we would expect that, at constant pulling speed, the cross-section area of the crystal would vary with the crystallization rate. This was indeed found to be true. If the melt temperature was decreased, and the rate of crystallization thereby increased, the cross-section area of the crystal would increase (and conversely).

However, it appears that the increases and decreases in cross-section areas are not fully reversible. It was found, on the one hand, that decrease of the melt temperature increased the thickness of the crystal, as well as its width. New planes would build up in the direction of the c-axis, as exhibited by the step growths. It should be noted that these steps start as hexagons; this indicates the preservation of hexagonal symmetry in the basal plane. On the other hand, when the temperature of the melt was increased, and the crystallization rate decreased, the corresponding decrease in cross-section area was manifested only in a decrease in the width of the crystal thickness.

A possible explanation for the observed behavior of the crystal shape is a general tendency toward masking anisotropic effects at high crystallization rates. This masking is represented by a transition from the flat shape to a more nearly cylindrical one; that is, to a thickening of the crystal. The ultimate cause of this thickening is probably the increased density of nucleation centers, produced by imperfections that occur when the crystal growth is rapid. But when the melt temperature is increased and the crystallization rate is thereby reduced, existing crystal planes probably tend to perpetuate themselves. Hence the only way that a decrease in the cross-section area can occur is by a decrease in the width of the crystal.

Approximately 0.5 gram of material condensed on the walls of the chamber, the crucible, and the seedholder during a run. At first, we thought that this material was tellurium alone because its vapor pressure was higher than that of bismuth, at least at room temperature. However, a chemical analysis (Manley 1960) has shown that this residue contains both bismuth and tellurium in approximately equal amounts. This finding is supported by the fact that crystals grown from stoichiometric melts all have very uniform properties; this indicates that the melt composition does not change much with time. For these stoichiometric crystals the resistivity, at room temperature, was approximately 1 milliohm-cm; the Hall constant, 0.40; and the thermoelectric power, approximately 215 $\mu$v/degree.

Attempts have been made to dope pulled bismuth telluride crystals with iodine. Because the particular apparatus employed here must be evacuated to eliminate oxygen, it is not feasible to dope by placing pure iodine in the pulling chamber because it would be pulled out of the system by the vacuum pump. The compound bismuth tri-iodide was

tried instead. It was found that if the $BiI_3$ was placed with the cold material in the crucible, it would decompose at a temperature lower than the melting point of $Bi_2Te_3$. The iodine vapors then etched the stainless-steel pushrod, and condensed both on it and on the chamber walls. Little iodine remained in the melt, the material was only slightly compensated, and it remained strongly p-type. The resistivity of the crystal pulled from such a doped melt was 2.3 milliohm-cm, the Hall constant at room temperature was 0.80, and the thermoelectric power 220 μv/degree (p-type).

To circumvent the decomposition problem, some $Bi_2Te_3$ was placed in a nickel container suspended in the chamber. After the melt was brought to equilibrium growing temperature, a magnet was used to dump the $BiI_3$ into the melt. The resulting crystal was n-type, with a thermoelectric power of −100 μv/degree, R = 0.79, and ρ = 5 milliohm-cm. There was sufficient dirt in the $BiI_3$ to cover a substantial portion of the melt and thus make it impossible to grow a very thick crystal.

Good iodine-doped crystals were finally obtained by adding to 120 grams of stoichiometric material 60 grams of iodine-saturated material reacted in a Bridgman furnace. The first crystals pulled from this melt had a thermoelectric power of −120 μv/degree and the third crystal, −216 μv/degree with a Hall constant of 0.38. The first crystals had too much iodine. During these pullings enough iodine escaped so that the third crystal had the right amount to give nearly the maximum thermoelectric power that occurs in this material. These crystals were 2.9 mm thick.

## 3.3 CUTTING OF SINGLE CRYSTALS OF $Bi_2Te_3$

Bismuth telluride is a very brittle material with well-defined cleavage planes. It is therefore very hard to work. Several methods for cutting it without damage were tried.

If a smooth cut surface is not of great importance, sandblasting is the quickest method. The crystal to be cut is affixed to a microscope slide with a 1-mm coating of rosin. This slide is moved in a micromanipulator under the sandblast. Cuts can be made this way through a 1 cm × 2 mm crystal in approximately 5 minutes. The drawback of this method is that pits are formed in the sample, apparently from vortices in the sandblast (Fig. 3.3-1). These vortices begin to form at distances approximately 1 mm from the nozzle of the blaster. Cuts free from pits can be made if the total thickness of the sample, including the potting material, is less than approximately 1 mm. This method has been used to cut the samples for the thermoelectric-power and Hall-effect determinations to be reported in Chapter IV.

The damage produced by this cutting procedure was evaluated by making it visible by etching the sample in a 2:1 solution of aqua regia for 10 minutes. All cracks were

(a)

(b)

Fig. 3.3-1. $Bi_2Te_3$ crystals cut by the sandblaster.

clearly displayed after the treatment. A sample with a crack is shown in Fig. 3.3-1b. Nearly all of the samples were crack-free.

# CHAPTER IV

# MEASUREMENTS OF THERMOELECTRIC POWER, CONDUCTIVITY, AND HALL EFFECT OF $Bi_2Te_3$

## 4.1 APPARATUS FOR MEASURING THERMOELECTRIC POWER

The usual way to make thermoelectric-power measurements is to embed thermocouples in the sample and apply the thermal difference at the ends of the sample. In this way, the potentials and the respective temperatures are measured at exactly the same points.

However, the grown $Bi_2Te_3$ crystals have a maximum thickness of approximately 2.9 mm perpendicular to the c-axis and measurements must be made with the heat flow both parallel and perpendicular to this axis. With this small thickness it is impractical to embed thermocouples in the sample because they would cause a very large perturbation in the heat flow.

The apparatus was designed to permit measurement with thermocouples attached to the contacts, which were either soldered or glued to the sample with silver paint. With this apparatus there exists the possibility of thermal gradients in the contacts so that the thermocouples would measure a higher temperature difference than was actually applied to the sample. If this were the case, the value of thermoelectric power obtained could depend on the temperature gradient applied. When solder was used to mount the samples the thermoelectric-power readings were completely independent of temperature differences from 3°C up to approximately 25°C. Below this temperature, the accuracy is limited by the accuracy of the potentiometer, and above it the variation of thermoelectric power with temperature (approximately 0.25 μv/degree) of the material becomes significant. When silver paint was used to mount the sample the readings were approximately 3 per cent low and a variation of thermoelectric power with temperature gradient became perceptible for a $\Delta T$ of approximately 20°C. Pressure mounting of the sample resulted in readings that were 25 per cent low and very temperature-gradient dependent.

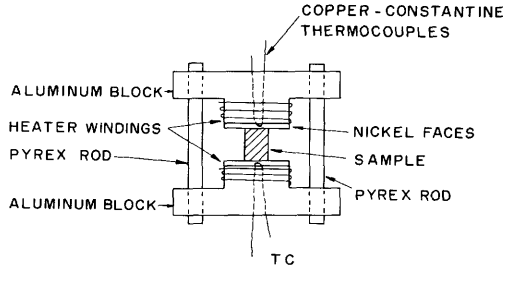


Fig. 4.1-1. Apparatus for measurement of thermoelectric power.

A diagram of the apparatus is shown in Fig. 4.1-1. The thermocouples were insulated from the aluminum block with thin drawn glass tubing. The anodyzing was found to be unreliable for insulation. At first, ceramic thermocouple tubing was used but the reading varied greatly with $\Delta T$. The reason for this was that the ceramic insulated the thermocouple thermally from the aluminum block. Heat was carried away by the thermocouple

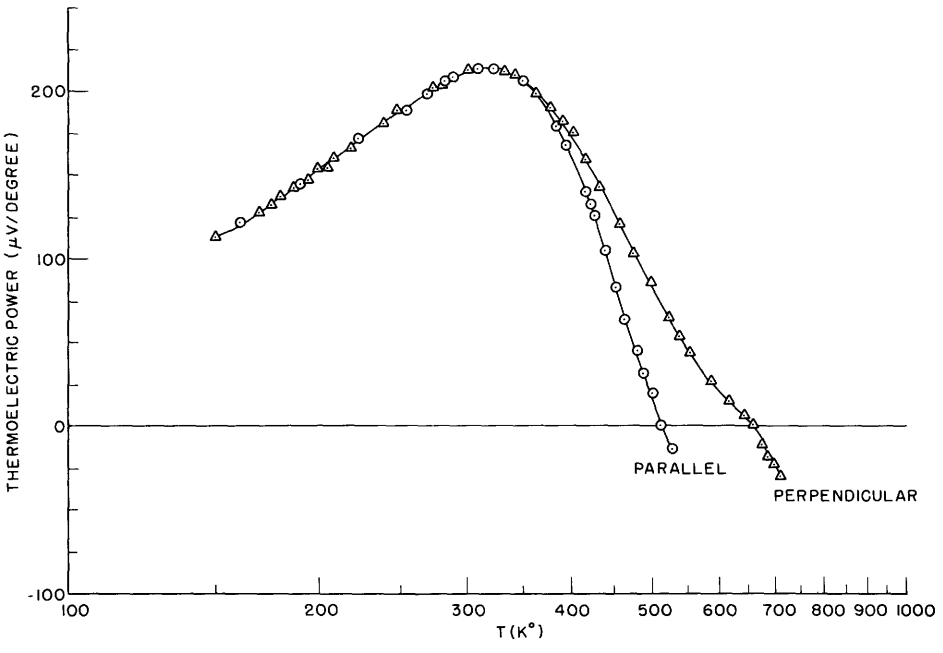


Fig. 4.1-2. Thermoelectric power versus temperature for stoichiometric p-type $Bi_2Te_3$.

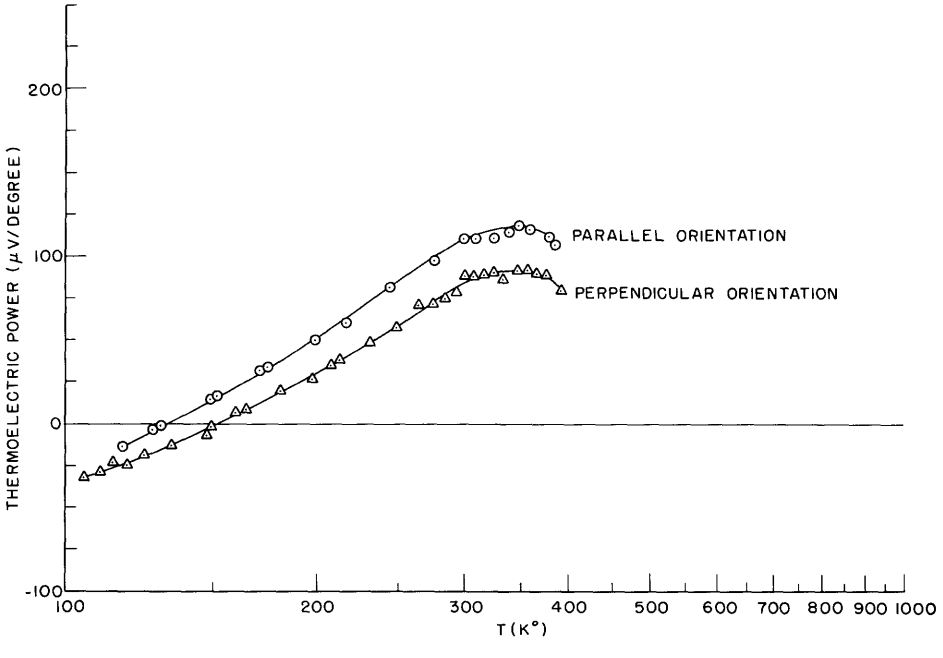


Fig. 4.1-3. Thermoelectric power of n-type $Bi_2Te_3$.

wires, hence the bulb of the thermocouple was at a lower temperature than the actual sample surface. This situation resulted in high readings of thermoelectric power. When the ceramic tubing was replaced by thin-walled glass the readings became independent of temperature gradient.

The heater windings were of an oxide-insulated cupro-nickel wire wound on Fiberglas tape. There are two identical windings on the two blocks with an additional temperature-gradient winding on one of them. The heater windings had a resistance of approximately 1 Ω and were powered by 6.3-volt filament transformers driven by variacs.

Solder was used for the contacts from 100°K to 390°K. Above this temperature, the indium solder melted and quickly destroyed the sample by forming an alloy with it. Use of high-temperature solders such as lead tin resulted in cracking of the sample when it cooled. Silver paint was tried from 320°K to 700°K. The results were consistent up to 500°K on samples that were cut parallel to the cleavage planes, and up to 650°K on samples that were cut perpendicular to the cleavage planes. At these points the samples became discontinuously n-type; this indicated doping by the silver in the paint. At 650°K the silver paint charred, leaving a poor mechanical contact when the sample was returned to room temperature. The reason that the parallel orientation became contaminated at a lower temperature than the perpendicular orientation is that silver will diffuse along the planes more readily than it will across the planes.

The thermoelectric power of stoichiometric samples of both orientations is shown in Fig. 4.1-2, and the thermoelectric power of iodine-doped material in both orientations is shown in Fig. 4.1-3.

## 4.2 MEASUREMENT OF CONDUCTIVITY OF $Bi_2Te_3$ FROM LIQUID-NITROGEN TEMPERATURE TO ROOM TEMPERATURE

The conductivity of both p-type and n-type materials in both orientations was measured by an ac method. A Hewlett-Packard 300C oscillator was used to drive a 60-watt McIntosh amplifier that supplied approximately 0.5 amp to the sample through an 8-ohm resistor. The voltage was measured across probes of 0.005-inch gold wire by a General Radio wave analyzer. The measurement was made at 275 cps.

For parallel samples, soldered end contacts were used and the voltage probes, in some cases, were soldered by potting the sample in a thin vat of rosin, sandblasting two parallel narrow grooves across the thickness and perpendicular to the length of the sample, nickel-plating the groove, and soldering to the nickel plate with Cerroseal. In other cases, the voltage probes were sparked with a low-voltage (7-volt) high-capacity (20,000 mfd) spot welder. Although strain lines were visible when the sparked contacts were used, the results were substantially the same as those with the solder contacts.

The perpendicular samples were only 2.9 mm thick, making soldered voltage probes, which were seldom less than 0.5 mm wide, impractical. Sparked contacts were used. Whenever soldered end contacts were used for the perpendicular orientation the

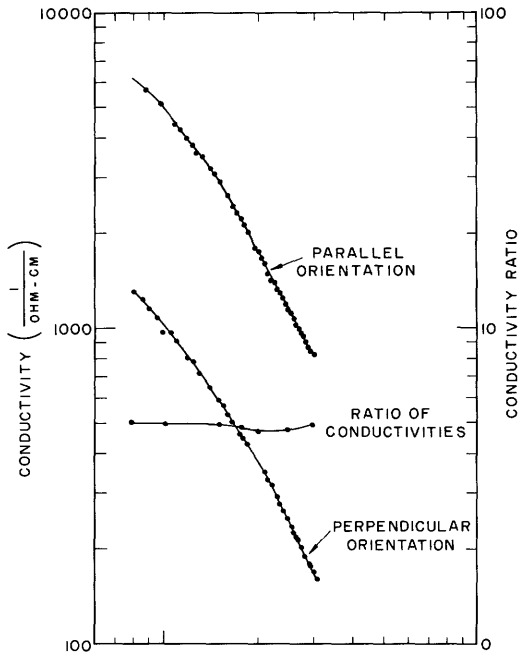


Fig. 4.2-1. Conductivity and conductivity ratio of p-type $Bi_2Te_3$.

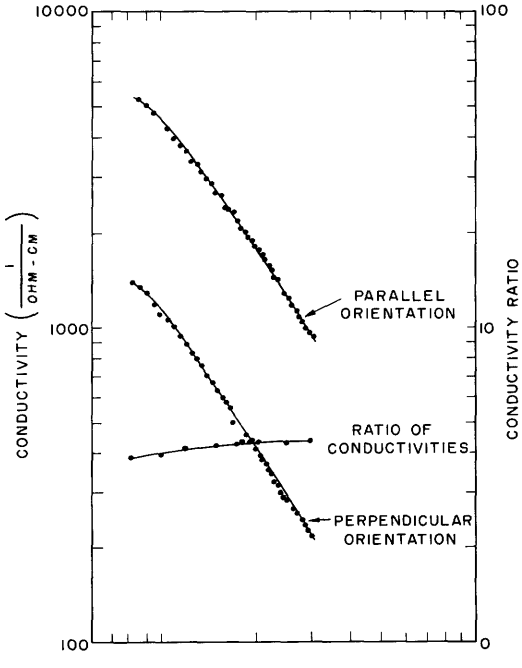


Fig. 4.2-2. Conductivity and conductivity ratio of n-type $Bi_2Te_3$.

values of conductivity obtained were lower than predicted by the theoretical value of $\sigma_{\parallel}/\sigma_{\perp}$; thus damage to the sample was indicated. The ends of the sample were nickel-plated and pressure contacts were used to pass current through the sample. The ends of these samples were quite parallel because of the nature of the crystal, but the edges were very ragged because of the rough cuts made by the sandblaster. The absolute value of the conductivity is therefore quite uncertain.

The conductivity and conductivity ratio of p-type samples for both orientations are shown in Fig. 4.2-1, and for n-type samples in Fig. 4.2-2.

## 4.3 SIMPLIFIED MEASUREMENT OF HALL EFFECT AT ROOM TEMPERATURE

The carrier concentration in $Bi_2Te_3$ is very large (approximately $10^{19}$ per cubic centimeter). Therefore the Hall voltage is very small (approximately 10 μv) for samples of manageable thickness (0.5 mm). Direct-current measurements are complicated by interfering thermal effects, but it was found that Hall voltages could nevertheless be measured with an accuracy of 10 per cent if these effects were properly taken into account (Lindberg 1952). Values thus obtained were found to check with ac measurements made on the $a\rho$ equipment (AFCRC-TN-60-125) within the stated accuracy.

The dc apparatus consisted of a modified magnetron permanent magnet, immersed in a large water tank. The sample was suspended in the water between the poles. The field was reversed simply by turning the sample around. The water tank and sample support rested on a large stack of newspapers that reduced the vibration markedly. The water served to minimize thermal effects, especially those usually produced by drafts. Current was supplied by a storage battery and a series resistor. The Hall voltage was measured directly with a Kiethley micro voltmeter. With this meter it was possible to see the drifts in readings caused by the thermal effects.

Undoped stoichiometric p-type samples cut from pulled crystals had a Hall constant of 0.4 and resistivity of 1 milliohm-cm along their cleavage planes. Partially compensated p-type iodine samples had a Hall constant of approximately 0.8 and resistivity of 4 milliohm-cm. The n-type iodine-doped crystals made with iodine-saturated Bridgman material had a Hall constant of 0.4.

# CHAPTER V

# COMPARISON OF THEORY WITH EXPERIMENT

## 5.1 CHECK ON THE VALIDITY OF THE THEORY OF THERMOELECTRIC POWER BASED UPON MIXED CONDUCTION AND A SINGLE SCATTERING MECHANISM

The validity of the theory of thermoelectric power based upon mixed conduction and a single scattering mechanism has been checked in a number of ways.

The detailed behavior of both orientations was checked on bismuth as we have described it in section 2.11. In bismuth telluride the effect can only be observed at high temperatures at which measuring techniques are difficult, and so a complete quantitative check was not made because of lack of complete data. Nevertheless, by using our thermoelectric-power data, which does not extend all the way up to the intrinsic range, a qualitative check of the anisotropy was made and the results reported in section 5.121.

In section 5.122 the conductivity and Hall data of Shigetomi and Mori (1956), on the parallel orientation only, was used to compute curves of thermoelectric power as a function of temperature in the transition range. The computed curve for the parallel orientation is then compared with their experimental thermoelectric-power data on the same orientation. The agreement of the calculated curve with the experimental points is good up to the knee of the transition range, but not beyond. The calculated curve for the other orientation is discussed qualitatively.

In section 5.123 the limiting values of the thermoelectric powers in the intrinsic range are computed by a method that is completely independent of the data of Shigetomi and Mori that were used in section 2.122 and is based on the energy-gap value given by Goldsmid. Qualitative agreement with the published value of the intrinsic thermoelectric power in the parallel direction is good. There are, to our knowledge, no published data on intrinsic thermoelectric power for the perpendicular orientation, but consistency with other data is considered.

### 5.11 Bismuth

The first check on the validity of the two-carrier single-scattering mechanism theory of thermoelectric power was made on bismuth by Chandrasekhar (1959). The model used by Abeles and Meiboom to interpret magnetoresistance data on bismuth comprises a conduction band having six ellipsoids (this band model is identical with the one that we used on bismuth telluride, which has a crystal structure identical with that of bismuth), and a two-ellipsoid valence band. Our six-ellipsoid model for the valence band of bismuth telluride can be reduced, of course, to the two-ellipsoid model by setting $s = 0$ and dividing by 3 in the valence-band parts of Eqs. 2.5-3 and 2.5-4. Chandrasekhar used the thermoelectric-power expression involving the mobility ratio (our Eq. 2.5-4) with the magnetoresistance data of Abeles and Meiboom to obtain the density-of-state effective

masses for bismuth. His value for this effective mass for the electrons agrees well with that deduced from the de Haas-Van Alphen effect and cyclotron resonance experiments. The value for holes is very close to that given by cyclotron resonance, but much smaller than is inferred from electronic heat-capacity data. We have checked Chandrasekhar's calculation independently, but happen to have done so in reverse, by calculating the values at room temperature of the thermoelectric power from the above-mentioned effective masses. We have accordingly achieved good agreement with his published data on thermoelectric power. We also measured the thermoelectric power of bismuth at room temperature in the two orientations and found it to be in close agreement with the theory. In addition, we made the same measurement on a single-crystal sample of antimony and found the thermoelectric power to be approximately 20 μv/degree with heat flow along the c-axes, and 40 μv/degree with heat flow in the cleavage planes. We have not made calculations on antimony.

## 5.12 Bismuth Telluride at High Temperatures

### 5.121 Qualitative Agreement with the Theory of Anisotropy in the Transition Range

We have used the effective mass and conductivity values of Drabble et al. to compute the $\gamma$ parameter of Eq. 2.5-13 for the two principal directions. The calculation is given in Appendix A. The value of $\gamma_\perp$ is greater than that of $\gamma_\parallel$; thus the thermoelectric power should be more p-type in the perpendicular direction (current flow perpendicular to the cleavage planes) than it is in the parallel direction (current flow along cleavage planes). This prediction is in qualitative agreement with the data illustrated in Fig. 4.1-2 which is isotropic at low temperatures, when conduction is by a single carrier, and becomes increasingly anisotropic when mixed conduction sets in. This anisotropy increases with temperature as the number of electrons becomes more nearly comparable to the number of holes. Just before contamination of the samples by the contacts the two curves appeared to be beginning to level off toward their intrinsic values.

### 5.122 Quantitative Agreement of Thermoelectric Power with Theory and Qualitative Agreement of $TEP_\perp$ with Theory in the Transition Range with the Use of the Data of Shigetomi and Mori

A curve of thermoelectric power versus temperature can be calculated directly if the Fermi level is known as a function of temperature. This level can be obtained from the equations

$$F_{1/2}(\eta_e) = \frac{nh}{2\left(\pi m_e^* kT\right)^{3/2}}$$

and

$$F_{1/2}(\eta_h) = \frac{ph}{2\left(2\pi m_h^* kT\right)^{3/2}}$$

These concentrations may be found from the conductivity and mobilities by means of the equations

$$n = p - p_s$$

and

$$\sigma = \mu_h e(bn+p)$$

when $p_s$ is the number of acceptors, and $b = \mu_e/\mu_h$ is assumed to be constant in the calculation.

The mobility of holes in the saturation range is found by dividing the conductivity by the number of acceptors: $\mu_p = \sigma/p_s$.

The values taken from a straight-line extension of the saturation-range conductivity curve divided by $p_s$ are assumed to give the mobility at high temperature. The number of acceptors is obtained from the Hall constant and its anisotropy factor $A^{(p)}$. Thus

$$R = \frac{r}{p_s e} A^{(p)}$$

where

$$r = \frac{(\tau^2)}{(\tau)^2}$$

The Hall "constant" is not constant but rises with temperature, its value at 300°K being 1.6 of its value at 77°K. Drabble's calculation of $A^{(p)}$ is made at 77°, so we shall make the computation of $p_s$ at this temperature. Our calculation is made from the data of Shigetomi and Mori. Their data are for a single-crystal specimen with the current flow along the cleavage planes. Their experimental points, along with our calculated points, are shown in Appendix C (Fig. C-2). Our calculated points for the perpendicular orientation are also shown.

The calculated points follow their experimental points quite well up to approximately 500°. Then the calculated curve levels off too soon. The reason for this behavior is that at high temperature the extrapolated mobility drops faster than $T^{-3/2}$, causing the $F_{1/2}(r)$ value to become large, in fact, large enough to give positive Fermi levels for both holes and electrons. This would imply the vanishing of the energy gap; this result is at variance with the data from other workers. It is possible that the mobility extrapolation does not hold at high temperatures, but it seems unlikely that the scattering mechanism would change from the 3/2 power law at high temperatures. It is more likely that the effective masses would change with the position of the Fermi level.

The thermoelectric power curve for the perpendicular orientation again behaves in a

manner that is qualitatively correct. It is coincident to the parallel curve in the region of one-carrier conduction, and separates from it, becoming more p-type than the curve for the parallel orientation when mixed conduction sets in. Finally, in the intrinsic range, the curve for perpendicular orientation appears to level off above the curve for parallel orientation.

### 5.123 Quantitative Agreement with Theory of Thermoelectric Power and Qualitative Agreement with Theory of Thermoelectric Power in the Intrinsic Range

It is also possible to calculate the intrinsic values of the thermoelectric power from the assumption that p = n, the values of the energy gap, and the mobility ratios. This is done in Appendix B. For the parallel orientation, the agreement with the experimental data of Goldsmid and of Shigetomi and Mori is quite good. They do not publish data for the perpendicular orientation. Our experimental thermoelectric-power data show that the perpendicular orientation is more p-type than the parallel orientation — which is the condition toward which our experimental curves seem to tend. Thus it is fair to say that the calculated values of intrinsic thermoelectric power in both orientations are consistent with the limited range of the available experimental data.

## 5.2 CHECK ON THE VALIDITY OF THE THEORY OF THERMOELECTRIC POWER BASED UPON SINGLE-CARRIER CONDUCTION AND A MIXED SCATTERING MECHANISM

The thermoelectric power of n-type iodine-doped $Bi_2Te_3$ is shown for both orientations in Fig. 4.1-3, the conductivity for both directions is shown in Fig. 4.2-2, and the ratio of conductivities is shown in Fig. 4.2-2. These data agree very closely with the results reported by Goldsmid. Our measurements were taken on pulled crystals, whereas his were taken on zone-refined material.

In Chapter II we derived a relationship between the anisotropy of thermoelectric power and the conductivity ratio, from Eq. 2.4-7. We obtained

$$TEP_{\parallel} - TEP_{\perp} = \frac{k}{e} \frac{d \ln\left(\frac{\sigma_3}{\sigma_1}\right)}{d(\ln kT)}$$

The slope of the plot of $\ln \frac{\sigma_3}{\sigma_1}$ versus $\ln kT$, from Fig. 4.2-2, is equal to 0.25. The difference of thermoelectric powers predicted by Eq. 2.4-7 is, then,

$$TEP_{\parallel} - TEP_{\perp} = 88\ \mu v/\text{degree} \times 0.25 = 22\ \mu v/\text{degree}$$

The maximum experimental difference between $TEP_{\parallel}$ and $TEP_{\perp}$ observed in Fig. 4.1-3 is 25 μv/degree, and is at the high-temperature end of the plot. This difference decreases as the temperature decreases. This can be explained as follows.

In the degenerate limit the thermoelectric power equals zero and, of course, the difference is zero. In the region of partial degeneracy the difference between the thermoelectric powers decreases (experimentally, as shown in Fig. 4.1-3) at about the same rate (with temperature) as the absolute value of the thermoelectric power decreases. The change in this difference is due to the increasing degeneracy.

## APPENDIX A

## COMPUTATION OF THE PARAMETER $\gamma$ OF EQ. 2.5-13

From the data of Drabble et al. (1956;1958) the density-of-states effective masses are

$$m_e^* = 0.45 \qquad \left(m_e^*\right)^{3/2} = 0.302 \qquad \left(\frac{m_h^*}{m_e^*}\right)^{3/2} = 1.22$$

$$m_h^* = 0.511 \qquad \left(m_h^*\right)^{3/2} = 0.368$$

Their three n-type samples are not radically different from one another. Our computation will be based on their n-type sample No. 19. The parameters at 77°K are:

$$\rho_{11} = 1.46 \times 10^{-6}$$

$$\frac{\rho_{33}}{\rho_{11}} = 4.1$$

$$A^e = 0.326$$

$$\rho_{123} = 0.425$$

The Fermi level is not available for this sample; r will be taken to be 1 at 77°K. Then

$$\rho_{123} = \frac{r}{ne} A^e$$

It follows that

$$ne = \frac{rA^e}{\rho_{123}} = \frac{0.326}{0.425 \times 10^{-6}} = 0.767 \times 10^6$$

The mobilities (in mks units) are:

$$\mu_{e_{\parallel}} = \frac{1}{\rho_{\parallel} ne} = \frac{1}{1.46 \times 10^{-6} \times 0.767 \times 10^{-6}} = 0.893$$

and

$$\mu_{e_{\perp}} = \frac{1}{\rho_{\perp} ne} = \frac{1}{4.1 \rho_{\parallel} ne} = 0.218$$

Their two p-type samples were quite different from each other. We shall make the calculation for both of them. The parameters at 77°K (in mks units) are:

| Parameters | Sample No. 19 | Sample No. 23 |
|---|---|---|
| $\rho_{11}$ | $4.23 \times 10^{-6}$ | $1.40 \times 10^{-6}$ |
| $\frac{\rho_{33}}{\rho_{11}}$ | 2.81 | 3.16 |
| $\rho_{123}$ | $1.06 \times 10^{-6}$ | $0.240 \times 10^{-6}$ |
| $A^p$ | 0.475 | 0.425 |
| r | 1.08 (from TEP) | |

The thermoelectric power of sample No. 19 was measured, and the Fermi level found to be +1.8. The computed value of r for this Fermi level is 1.09. No thermoelectric power data were available on sample No. 23, so we shall take r to be 1. We can now compute $p_e = \frac{rA^p}{\rho_{123}}$; the computation yields:

For sample No. 19,

$$\frac{1.08 \times 0.475}{1.06 \times 10^{-6}} = 0.485 \times 10^6$$

For sample No. 23,

$$\frac{1 \times 0.425}{0.24 \times 10^{-6}} = 1.77 \times 10^6$$

The mobilities (in mks units) are:
For sample No. 19,

$$\mu_{\rho_{\parallel}} = \frac{1}{\rho_{\parallel} p_e} = \frac{1}{4.23 \times 0.485} = 0.487$$

$$\mu_{\rho_{\perp}} = \frac{0.487}{2.81} = 0.173$$

For sample No. 23,

$$\mu_{\rho_{\parallel}} = \frac{1}{1.4 \times 1.77} = 0.403$$

$$\mu_{\rho_{\perp}} = \frac{0.403}{3.16} = 0.128$$

The mobility ratios are:
For sample No. 19,

$$\left(\frac{\mu_\rho}{\mu_e}\right)_{\parallel} = \frac{0.487}{0.843} = 0.545$$

$$\left(\frac{\mu_\rho}{\mu_e}\right)_\perp = \frac{0.173}{0.218} = 0.795$$

For sample No. 23,

$$\left(\frac{\mu_\rho}{\mu_e}\right)_{||} = \frac{0.403}{0.893} = 0.450$$

$$\left(\frac{\mu_\rho}{\mu_e}\right)_\perp = \frac{0.128}{0.218} = 0.589$$

The $\gamma$ parameters are: $\gamma_{||} = 0.545 \times 1.21 = 0.66$ for sample No. 19, and $0.450 \times 1.21 = 0.545$ for sample No. 23; $\gamma_\perp = 0.795 \times 1.21 = 0.961$ for sample No. 19, and $0.588 \times 1.21 = 0.712$ for sample No. 23.

## APPENDIX B

## CALCULATION OF THE INTRINSIC VALUES OF THERMOELECTRIC POWER OF $Bi_2Te_3$

In order to obtain the thermoelectric power, we must obtain the Fermi levels that are contained in the following expressions.

$$F_{1/2}(\eta_e) = \frac{nh}{2\left(2\pi m_e^* kT\right)^{3/2}}$$

$$F_{1/2}(\eta_h) = \frac{ph}{2\left(2\pi m_h^* kT\right)^{3/2}}$$

Now, if the material is intrinsic, n = p, which implies that

$$F_{1/2}(\eta_e) = \left(\frac{m_h^*}{m_e^*}\right)^{3/2} F_{1/2}(\eta_h) \tag{B-1}$$

and

$$kT\eta_e = E_f - E_c$$

$$kT\eta_h = E_v - E_f$$

and so

$$(\eta_e + \eta_h) = \frac{E_v - E_c}{kT} = -\frac{E_g}{kT} \tag{B-2}$$

The energy gap is a function of temperature. This temperature dependence can be expressed approximately as a linear perturbation from the value of the gap at absolute zero. The expression for it is

$$E_g = E_{g_o} + \beta T$$

Goldsmid (1957) gives the values

$$E_{g_o} = 0.16 \text{ ev}$$

$$\beta = -1.5 \times 10^{-4} \text{ ev/°K}$$

The melting point of the material is 58°C, which is 859°K. We shall arbitrarily pick T = 800°K to make this calculation. At this temperature the energy gap is 0.04 ev.

Now we must find, from the tables of McDougall and Stoner (1938), values of $\eta_e$ and

$\eta_p$ that simultaneously satisfy Eqs. B-1 and B-2. A good starting value would be the classical value given by

$$\eta_e = -\frac{1}{2}\frac{E_y}{kT} + \frac{1}{2}\ln\left(\frac{m_h^*}{m_e^*}\right)^{3/2}$$

$$= -\frac{1}{2}\frac{0.04}{0.0665} + \frac{1}{2}\ln 1.21$$

$$= -0.300 + \frac{0.19}{2} = -0.205$$

$$\eta_h = -\frac{E_y}{kT} - \eta_e$$

$$= -0.600 + 0.205$$

$$= -0.400$$

From the tables, if $\eta_h = -0.4$ and $\eta_e = -0.2$, then $F_{1/2}(\eta_h) = 0.489$ and $F_{1/2}(\eta_e) = 0.577$, and therefore

$$\frac{F_{1/2}(\eta_e)}{F_{1/2}(\eta_h)} = 1.18$$

Equation B-1 states that for classical statistics

$$\frac{F_{1/2}(\eta_e)}{F_{1/2}(\eta_h)} = \left(\frac{m_h^*}{m_e^*}\right)^{3/2} = 1.21$$

so classical statistics give a fairly good number at this temperature. Then it should be all right to use the classical formula for thermoelectric power given by Johnson and Lark-Harovitz (1953):

$$TEP = -\frac{k}{e}\frac{\left(1 - \frac{\mu_h}{\mu_e}\right)}{\left(1 + \frac{\mu_h}{\mu_e}\right)}\left(\frac{E_g}{2kT} + 2\right)$$

Using the values $\left(\frac{\mu_h}{\mu_e}\right)_{\parallel} = 0.545$ and $\left(\frac{\mu_h}{\mu_e}\right)_{\perp} = 0.795$ for sample No. 19, given in Appendix A, we obtain

$$\frac{\left(1 - \frac{\mu_h}{\mu_e}\right)}{\left(1 + \frac{\mu_h}{\mu_e}\right)} = 0.114$$

and therefore

$$TEP_{\parallel} = -88 \times 0.288(2.3) = -58 \ \mu v/\text{degree}$$

and

$$TEP_{\perp} = -88 \times 0.114(2.3) = -23 \ \mu v/\text{degree}$$

The value for $TEP_{\parallel}$ is in very good agreement with the published data of Shigetomi and Mori (1956) and of Goldsmid (1957). There are, to our knowledge, no published data for $TEP_{\perp}$.

## APPENDIX C

## CALCULATION OF THERMOELECTRIC POWER VERSUS TEMPERATURE IN THE TRANSITION RANGE

The conductivity data of Shigetomi and Mori (1956) are replotted on a log $\sigma$ versus log T scale in Fig. C-1. The low-temperature slope is extended into the high-temperature region. This extended curve divided by the number of acceptors is taken to be the mobility. The ordinates read from this curve are designated $\sigma_\mu$.

The Hall constant of this material at low temperatures, taken from Shigetomi and Mori's Hall curves, is 0.422. The number of acceptors is then given by

$$p_s = \frac{rA^p}{\rho_{123}e} = 0.75 \times 10^{19} \text{ per cubic centimeter}$$

when r is taken to have its classical value, and $A^p = .45$ is an average of the values for samples No. 19 and No. 23 of Drabble et al. (1956;1958). Data taken from Shigetomi and Mori's conductivity curve and the mobility extension of the conductivity curve, together with tabulated values of the Fermi integrals, have been used for the calculation described in Chapter V. The results are tabulated in Table I. The thermoelectric-power data of Shigetomi and Mori are replotted in Fig. C-2. Their points are represented as crosses. Our calculated points for the parallel orientation are shown as

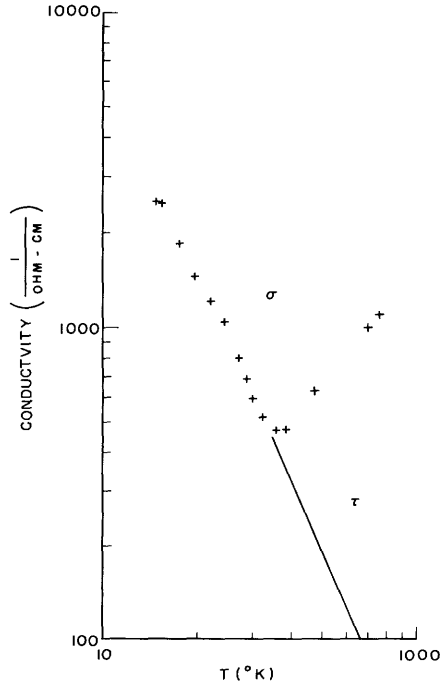


Fig. C-1. Replot of the conductivity data of Shigetomi and Mori.

Table I. Calculation of thermoelectric power of $Bi_2Te_3$ in the transition range.

| Point | T(°C) | T(°K) | $\sigma$ | $\sigma_\mu$ | $\frac{\sigma}{\sigma_\mu} p_s$ ($\times 10^{19}$) | p ($\times 10^{19}$) | n ($\times 10^{19}$) | $T^{3/2}$ | $F_{1/2}(\eta_h)$ | $F_{1/2}(\eta_e)$ |
|---|---|---|---|---|---|---|---|---|---|---|
| 1 | 26 | 300 | 593 | 593 | .75 | .75 | 0 | 5220 | .720 | .000 |
| 2 | 76 | 350 | 470 | 423 | .835 | .78 | .03 | 6580 | .593 | .0278 |
| 3 | 126 | 400 | 490 | 320 | 1.15 | .89 | .14 | 8000 | .555 | .107 |
| 4 | 176 | 450 | 595 | 250 | 1.79 | 1.11 | .36 | 9540 | .581 | .275 |
| 5 | 226 | 500 | 675 | 195 | 2.60 | 1.40 | .65 | 11,200 | .625 | .354 |
| 6 | 276 | 550 | 750 | 157 | 3.58 | 1.75 | 1.00 | 12,900 | .677 | .472 |
| 7 | 326 | 600 | 815 | 130 | 4.70 | 2.14 | 1.39 | 14,700 | .830 | .584 |
| 8 | 427 | 700 | 1000 | 9.1 | 8.25 | 4.06 | 3.31 | 18,500 | 1.38 | 1.37 |

| Point | $\eta_h$ | $\eta_e$ | $F_1(\eta_h)$ | $F_o(\eta_h)$ | $F_1(\eta_e)$ | $F_o(\eta_e)$ | $2\left(\frac{F_1F_{1/2}}{F_o}\right)_h$ | $2\left(\frac{F_1F_{1/2}}{F_o}\right)_e$ | $TEP_\parallel$ | $TEP_\perp$ |
|---|---|---|---|---|---|---|---|---|---|---|
| 1 | +.076 | $-\infty$ | .878 | .726 | - | - | - | - | +206 | +206 |
| 2 | -.167 | -3.8 | .714 | .612 | .0299 | .030 | 1.38 | .056 | +139 | +160 |
| 3 | -.248 | -2.1 | .659 | .576 | .118 | .114 | 1.27 | .221 | +85 | +124 |
| 4 | -.192 | -1.1 | .693 | .595 | .308 | .287 | 1.35 | .590 | +18.2 | +55 |
| 5 | -.100 | -.80 | .755 | .646 | .406 | .368 | 1.46 | .780 | -6.9 | +37 |
| 6 | .000 | -.40 | .822 | .693 | .582 | .511 | 1.61 | 1.08 | -20.2 | +21.3 |
| 7 | +.400 | -.20 | 1.14 | .911 | .693 | .596 | 2.04 | 1.33 | -25 | +12.1 |
| 8 | +1.00 | +1.00 | 2.30 | 1.32 | 2.30 | 1.32 | 4.78 | 4.78 | -61 | |

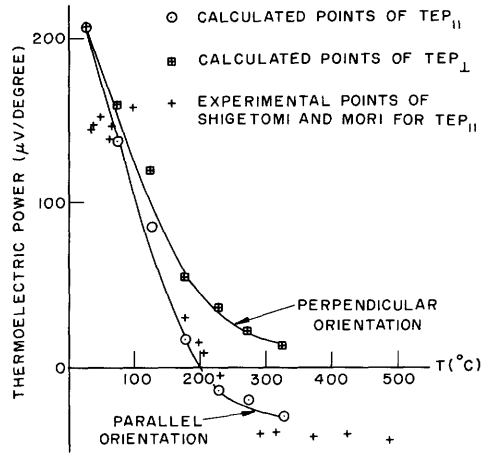


Fig. C-2. Thermoelectric power of $Bi_2Te_3$ in the transition range.

circles and those for the perpendicular orientation as squares.

The agreement of the calculated curve for the parallel orientation with the data of Drabble et al. and Shigetomi and Mori is quite good up to 300°C. Above that temperature, the n and p values obtained from the $\sigma$ and $\sigma_\mu$ curves give positive Fermi levels for both holes and electrons. This finding implies that the energy bands have overlapped and the material has become a semimetal. This is at variance with data of other workers. Apparently the mobility extrapolation is not good at these temperatures.

Acknowledgement

The author wishes to express her appreciation to her thesis supervisor, Professor Richard B. Adler for many stimulating discussions and much encouragement. Particular thanks are due to Professor Arthur C. Smith, for many stimulating discussions; to the thesis readers, Professor William P. Allis and Professor David C. White, for helpful criticism. Especial thanks are due to Professor Pierre Aigrain, of the Laboratoire Central des Industries Électriques, Fontenay-aux-Roses, France, who originally suggested the problem that is the subject of this thesis. I am grateful to my fellow-students Robert E. Nelson and Oscar P. Manley for many suggestions and encouragement. Many technological difficulties were solved with the aid of David A. Puotinen, and Henry J. Lawrence helped in the construction of the equipment.

The author would also like to express her thanks to the staff of the Research Laboratory of Electronics, M. I. T., who aided in many ways, in particular, to John B. Keefe and Fred Rosebury.

## Bibliography


AFCRC-TN-60-125. Theoretical and Experimental Research in Thermoelectricity. Scientific Report No. 1 on Contract AF19(604)-4153. Electronic Systems Laboratory, Massachusetts Institute of Technology, December 31, 1959.

Boydston, R. W. 1927. Thermo-electric effect in single-crystal bismuth. Phys. Rev. 30: 911-921.

Bullis, W. N. 1956. Galvanomagnetic Effects in n-Type Germanium. Ph. D. Thesis, Department of Electrical Engineering, Massachusetts Institute of Technology.

Chandrasekhar, B. S. 1959. J. Phys. Chem. Solids 11: 268-273.

Drabble, J. R. 1958. Galvanomagnetic effect in p-type bismuth telluride. Proc. Phys. Soc. (London) 72: 380-390.

Drabble, J. R. and Wolfe, R. 1956. Anisotropic galvanomagnetic effects in semiconductors. Proc. Phys. Soc. (London) B, 69: 1101-1108.

Drabble, J. R., Groves, R. D., and Wolfe, R. 1958. Galvanomagnetic effects in n-type bismuth telluride. Proc. Phys. Soc. (London) 71: 430-443.

Goldsmid, H. J. 1957. The Thermal Conductivity, Electrical Conductivity, and Thermal Power of Bismuth Telluride. Ph. D. Thesis, University of London. (Proc. Phys. Soc. (London), in press.)

Goldsmid, H. J. 1958. The electrical conductivity and thermal power of bismuth telluride. Proc. Phys. Soc. (London) 71: 633-646.

Johnson, V. A. and Lark-Horovitz, K. 1953. Theory of thermoelectric power in semiconductors with applications to germanium. Phys. Rev. 92: 226-232.

Lindberg, O. 1952. Hall effect. Proc. IRE 40: 1414.

Manley, O. P. 1960. Some Aspects of Copper Transport in Single Crystals of p-Type Bismuth. Ph. D. Thesis, Department of Electrical Engineering, Massachusetts Institute of Technology.

McDougall, J. and Stoner, E. C. 1938. The computation of Fermi-Dirac functions. Trans. Roy. Soc. (London) A237: 67-104.

Nye, J. F. 1957. Properties of Crystals. Oxford: Clarendon Press.

Satterthwaite, C. B. and Ure, R. W., Jr. 1957. Electrical and thermal properties of $Bi_2Te_3$. Phys. Rev. 108: 1164-1170.

Shepherd, F. D. 1959. Preparation of Single Crystals of $Bi_2Te_3$. S. M. Thesis, Department of Electrical Engineering, Massachusetts Institute of Technology.

Shigetomi, S. and Mori, S. 1956. Electrical properties of $Bi_2Te_3$. J. Phys. Soc. Japan 11: 915-919.

Shockley, W. 1950. Electrons and Holes in Semiconductors. New York: D. Van Nostrand Company, Inc.

Seitz, F. 1940. Modern Theory of Solids. New York: McGraw-Hill Book Company.

Wilson, A. H. 1953. Theory of Metals. London: Cambridge University Press.

Wyckoff, R. W. G. 1953. Crystal Structures. New York: Interscience Publishers (1948-1953).

Yates, B. 1959. The electrical conductivity and Hall effect in $Bi_2Te_3$. J. Electronics and Control 6: 26.